Cornelia Trummer, BSc

Preparation of Transmission Electron Microscopy Samples by Mechanical Techniques in Combination with Low-Voltage Ion Milling

MASTER'S THESIS

to achieve the university degree of

Diplom-Ingenieurin

Master's degree programme: Advanced Materials Science

submitted to

Graz University of Technology

Supervisor

Ao.Univ.-Prof. Dipl.-Ing. Dr.techn. Gerald Kothleitner

Institute of Electron Microscopy and Nanoanalysis

Graz, Mai 2017

AFFIDAVIT

I declare that I have authored this thesis independently, that I have not used other than the declared sources/resources, and that I have explicitly indicated all material, which has been quoted either literally or by content from the sources used. The text document uploaded to TUGRAZonline is identical to the present master's thesis dissertation.

____________________ ____________________________________

Date Signature

Abstract

For decades, samples for transmission electron microscopy analysis have been produced by standard mechanical pre-preparation like cutting, grinding, polishing, and dimpling with a subsequent broad argon ion milling step. But the progressive development of high-performance transmission electron microscopy needs a development of the sample preparation as well because it is one of the limiting factors for high-end TEM analysis down to the atomic scale. To generate a sample, which is only a few nanometers thin, with the least preparation artefacts, the thinning of the samples with focused low energy argon ions offers a viable way.

Practically it is very complicated to perform a low-energy argon ion milling of defined areas, especially on samples pre-prepared with this classical way after the first examination in a TEM. Therefore, we developed an elaborated preparation and analysis procedure as described in this thesis. To test this procedure, thinning was executed on different mechanical pre-prepared samples like planar, dimpled and cross-sectioned samples. For milling, a commercial low-energy thinning instrument called NanoMill® by Fischione Instruments was used in this thesis.

Another aim of this thesis was to characterise the milling behaviour of the equipment with the help of scanning electron microscopy and atomic force microscopy analysis, including the determination of the sputter rate of silicon at an incident angle normal to the silicon surface.

Based on the results of this study two novel preparation and examination procedures are given for improved thinning and cleaning of mechanically pre-prepared samples.

Acknowledgement

"Silent gratitude isn't much use to anyone" - G. B. Stern

First of all, I would like to thank Professor Ferdinand Hofer, head of our institute, for offering the possibility to write my thesis at the Institute for Electron Microscopy and Nanoanalysis. The ZFE, Center for Electron Microscopy, is given thanks for providing access to scientific infrastructure. I would also like to thank Professor Gerald Kothleitner for being my supervisor and for his scientific guidance through my whole work. I express my gratitude to Martina Dienstleder who supported me with all her possibilities during the whole master thesis and for giving me competent advice to bring my work to a successful completion. Moreover, I want to thank Evelin Fisslthaler for her pieces of advice. I would also like to thank Regina Seidl for helping me with the microscope and Jürgen Sattelkow spending his time with the AFM measurements.

Special thanks go to my office colleagues, improving my mood by making me laugh and having encouraging words for me. Besides that, I want to thank the whole FELMI-ZFE team, for the relaxing coffee breaks and amusing discussions.

Furthermore, I want to thank my boyfriend Walter, who told me, that I could create everything I imagine and I want to thank his whole family, promising me that all things end.

But my biggest hug and thanks I have to give to my family. They supported me throughout my whole life and gave me enormous backing and moral support during my master degree. They were always there when I needed them, and who were the first to believe in me. Thank you for being there for every time I needed you!

Table of Contents

1. Introduction and Motivation 1
2. Fundamentals 2
  2.1 TEM Sample Preparation 2
    2.1.1 Mechanical Sample Preparation 2
    2.1.2 Ion Milling Techniques 3
  2.2 Microscopy Methods 9
    2.2.1 Visible Light Microscopy 9
    2.2.2 Transmission Electron Microscopy 11
    2.2.3 Thickness Measurement – t/λ-Method 14
  2.3 Atomic Force Microscopy 17
3. Practical Work 19
  3.1 Sample Preparation - Overview 19
  3.2 Disc Preparation 21
  3.3 Sandwich Cross-section Preparation 24
  3.4 Wire Marker Preparation 25
  3.5 Conventional Ion Milling with the PIPS™ 27
  3.6 Low-Energy Ion Milling with the NanoMill® 28
4. Results 31
5. Atomic Force Measurements -Beam Characterization 55
6. Conclusion 65
  Bibliography .... A

Abbreviations

AFM	atomic force microscopy
BF	bright field
SED	secondary electron detector
EELS	electron energy loss spectrum/spectroscopy
EFTEM	energy filtered transmission electron microscopy
FIB	Focused Ion Beam system (by FEI, Nova200^{TM} Nanolab)
HRSTEM	high-resolution scanning transmission electron microscopy
keV	kilo electron volt
LIMI	light microscope
LE	Low-energy
mbar	millibar
mm	millimetre
nm	nanometre
PIPS^{TM}	Precision Ion Polishing System (by Gatan Inc.)
rpm	revolutions per minute
SEM	scanning electron microscopy
Si	silicon
SiC	silicon carbide
TEM	transmission electron microscope/microscopy
ZLP	zero-loss peak

1. Introduction and Motivation

The requirements for transmission electron microscopy (TEM) samples have increased through the years, because of the more efficient analysis equipment. Ideally, they shall be flat and smooth (without scratches), thin enough (under 50 nm) to be electron transparent and the material must be stable under the electron beam as well as robust against oxidation and environmental influences.[1], [2]
The NanoMill® by Fischione Instruments is a low energy (LE) argon ion milling device, which is used at the Institute of Electron Microscopy and Nanoanalysis for post-processing of focused ion beam (FIB) lamellae to reduce FIB induced artefacts. [3]– [5]
The use of this instrument can also be extended for low-voltage post treatments of conventionally prepared samples to enhance the quality of the sample [6]. This thesis sets the focus on the development of procedures for thinning mechanically prepared (cutting, grinding, polishing etc.) and pre-prepared and pre-milled by (PIPS™) samples. [1]
The LE milling device provides the possibility to reduce preparation artefacts, accompanied by a thickness reduction and ablation of amorphous layers [7] which is desirable for high-resolution scanning transmission electron microscopy (HRSTEM). Organic impurities on the surface can be removed as well. An important advantage of this kind of milling is the generation of a focussed ion beam, which makes it possible to thin a selected area of the sample. The analysis of the thickness reduction performed by the mill is done by relative thickness measurements (t/λ-method) in energy-filtering mode on the TEM CM20 by Philips [8]. To get an estimate of the sputter rates particularly for silicon, special test samples were created in a particular way so that the ion beam hits the sample normal to the sample surface (90°) with a source energy of 900 eV and 100 pA beam current. Atomic force microscopy (AFM) then, was thought to be able to measure the received sputter volume and to calculate sputter rates.

2. Fundamentals

This chapter gives general information about mechanical sample preparation, low-voltage ion milling techniques and microscopy methods, which are used in this master thesis.

2.1 TEM Sample Preparation

Classical preparation techniques used for TEM studies have the purpose to thin the sample in the form of a thin slice or a powder, whose thickness does not exceed 100 nm. Mechanisms involved in thinning can be of physical and chemical nature; most commonly they are based on mechanical methods or ablation by ion beams. A combination of different techniques is often necessary to obtain a thin and well-prepared sample. [1]

The goal in sample preparation for TEM analysis is simple in principle: the sample must be of a defined geometry and thickness (to fit in the electron microscope sample holder and be electron transparent), with a large area of equal thickness, artefacts should not be introduced during the preparation steps and it should be mechanically strong enough to withstand handling.[1], [9]

In addition, the process should be fast, reproducible and economic. The preparation technique itself may cause artefacts that influence the measurement. Depending on the material and its properties, different mechanical preparation methods can be used. For special demands, preparation techniques must be modified or new ones must be developed.[2], [10].

2.1.1 Mechanical Sample Preparation

The main methods, used for mechanical sample preparation in this master thesis are mechanical cutting (ultrasonic cutting), grinding, polishing, and dimpling. Silicon was used as a reference material, common to many technologically relevant material systems. All preparation techniques are described in detail in chapter *3*. Those techniques are used to reach a sample that can be additionally thinned down by means of ion milling [1]. Thinning of the sample with Ar^{+}-ions (PIPS™) to electron transparency and post-treatment on a low-voltage Ar^{+}-ion polishing system (NanoMill®) is employed to reduce preparation-induced artefacts. A short overview of ion milling techniques is given in the next subsection *2.1.2*.

2.1.2 Ion Milling Techniques

The principle of ion beam milling is based on the bombardment of the sample with energetic ions, which –due to impact- sputter material off its surface. This process takes place in a gas plasma. The utilised ions should be inert, heavy, inexpensive, and not present in the material, such as Argon. [1], [11].

The material is removed fast (by reason of higher sputter rates) from a large area at high voltage (> 2 keV) to optimise the sample thickness, but it may cause artefacts such as re-deposition, ion implantation and formation of an amorphous layer. [12]

Avoiding structural changes and cleaning a small sample surface area is then possible using a low-voltage ion milling device (NanoMill® from Fischione, GentleMill™ from Technoorg.). For the milling process low energy (900 eV) Argon ions are used. It decreases surface damage from previous preparation steps and enhances the sample quality. The chosen devices in this master thesis are described on the following pages in detail.

2.1.2.1 Precision Ion Polishing System, PIPS™

A standard tool, used for ion milling, is the Precision Ion Polishing System (PIPS™) from Gatan. The device and the view from above into the sample chamber is shown in *Figure 1*.

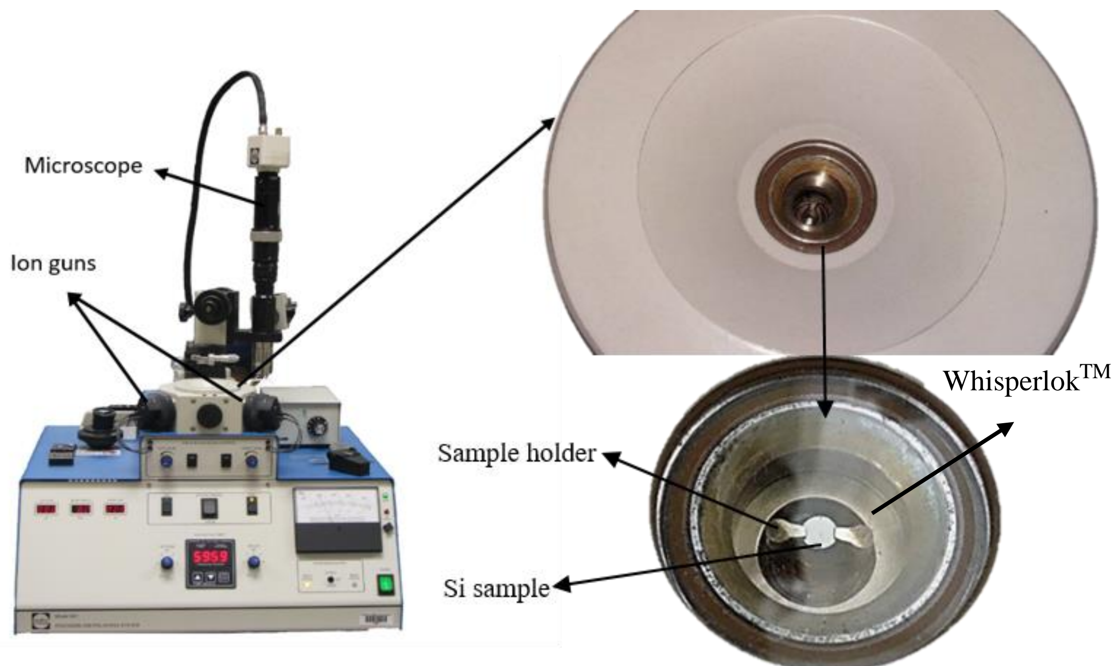

Figure 1: Design of the ion milling PIPS™ device (left) with sample holder and Whisperlok™ specimen transfer (right).

The aim of a Precision Ion Polishing System is ion milling of samples, which were pre-thinned down by previous mechanical sample preparation steps (see chapter *3*) like cutting, grinding, polishing and, if necessary, dimpling. The PIPS^{TM} uses a broad beam (> 0.01 µm) for ion milling. [2], [13]

The main components of a PIPS^{TM} are:

- Sample holder
- Sample transfer lock (Whisperlok^{TM})
- Vacuum system
- Ion guns/Beam modulation

The sample holder is a PIPS^{TM} "Aluminum DuoPost^{TM}" clamp type, which is perfect to grip the sample at its outer edge. The Whisperlok^{TM} system eliminates the need to vent the whole vacuum chamber and due to that, a quick exchange of the sample is possible. A molecular drag pump, backed with a diaphragm pump, is used to produce the vacuum in the chamber. By the impact of Ar^+-ions, accelerated by an electric field and focused at a certain position, the material can be removed. Holes are produced, and at their edge regions, the sample is electron transparent. Ion thinning, which is possible for materials like ceramics, semiconductors and metals, takes place in a vacuum. A beam modulation provides the option to thin the sample from one side or both. In order to thin from both sides, (*Figure 2*) two separate ion guns generate Ar^+-ions, with energies between 0.1 keV and 8 keV and in adaptable angles from 0 to 10°. [2], [13]–[15]

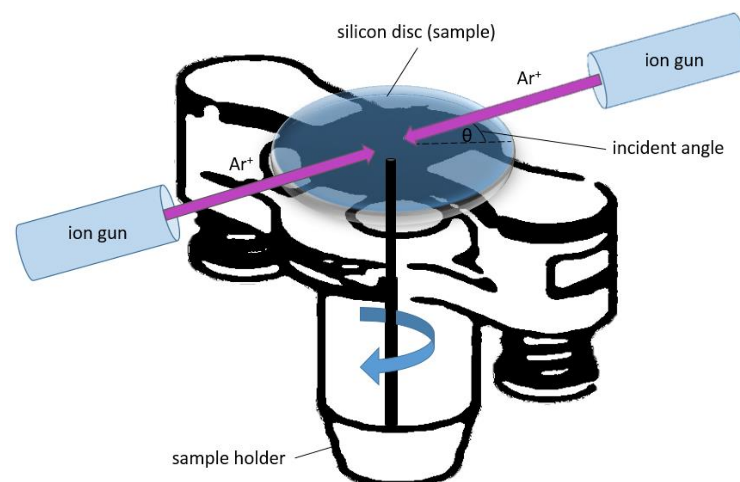

Figure 2: Schematic image of the two-sided ion milling beam modulation, which provides the option to thin a sample double-sided. (modified from [15])

The milling rate is influenced by the following parameters:

- Relative masses of the ion and sample atom
- Ion energy
- Atomic density
- Crystalline structure of the sample
- Incidence angle of the ion beam

As a rule, the higher the beam energy and the beam angles are, the faster is the milling rate. Higher energy and angles lead to more damage on the sample surface.[6]
These amorphous layers depend on the material and milling parameters. PIPS^{TM} thinning routinely leads to samples with larger electron transparent areas with a thickness below 100 nm. However, there is a linear dependence between the incident angle and the thickness of the amorphous layer as well as between the acceleration voltage and layer thickness [16].

2.1.2.2 NanoMill®

For high-resolution TEM analysis, samples should be ultra-thin and as artefact-free as possible. For this, only PIPS™ thinning is not enough. A low energy (down to 50 eV) Ar^+-ion milling device, Fischione's Model 1040 NanoMill® (see *Figure 3*) is used after PIPS™ thinning to get high-quality thin samples.

A focused ion beam with the minimum beam diameter of 2 µm allows to target and thin a selected area of the sample with the positive side effect, that damaged layers are removed from the surface without redeposition. The targeting is done through a user interface, by observing a secondary electron image. [4], [6]

The device consists of seven essential parts:

- Ion beam source
- Vacuum chamber and pumps
- Load lock
- Sample stage
- Cooling system
- Secondary electron detector
- Faraday cup

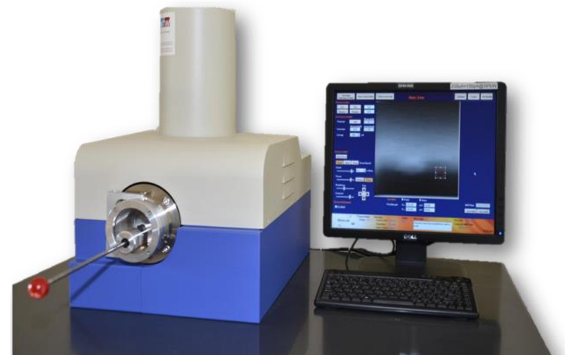

Figure 3: Model 1040 NanoMill® with user interface on computer screen. [8]

It includes an electron impact device to generate Ar^+-ions by bombarding the neutral argon gas with electrons. The latter come from a yttrium-coated iridium disc filament. The created ions are accelerated at low voltages from 50 to 2000 eV. When ions are focused to a certain position of the sample, secondary electrons are generated. On the one hand, electrons are used to remove atoms from the surface of the materials and on the other hand, electrons are used for imaging. A secondary electron detector (SED) detects the latter. [17]

A big disadvantage of the instrument is shown in *Figure 4* by comparing three images taken at different acceleration voltages.

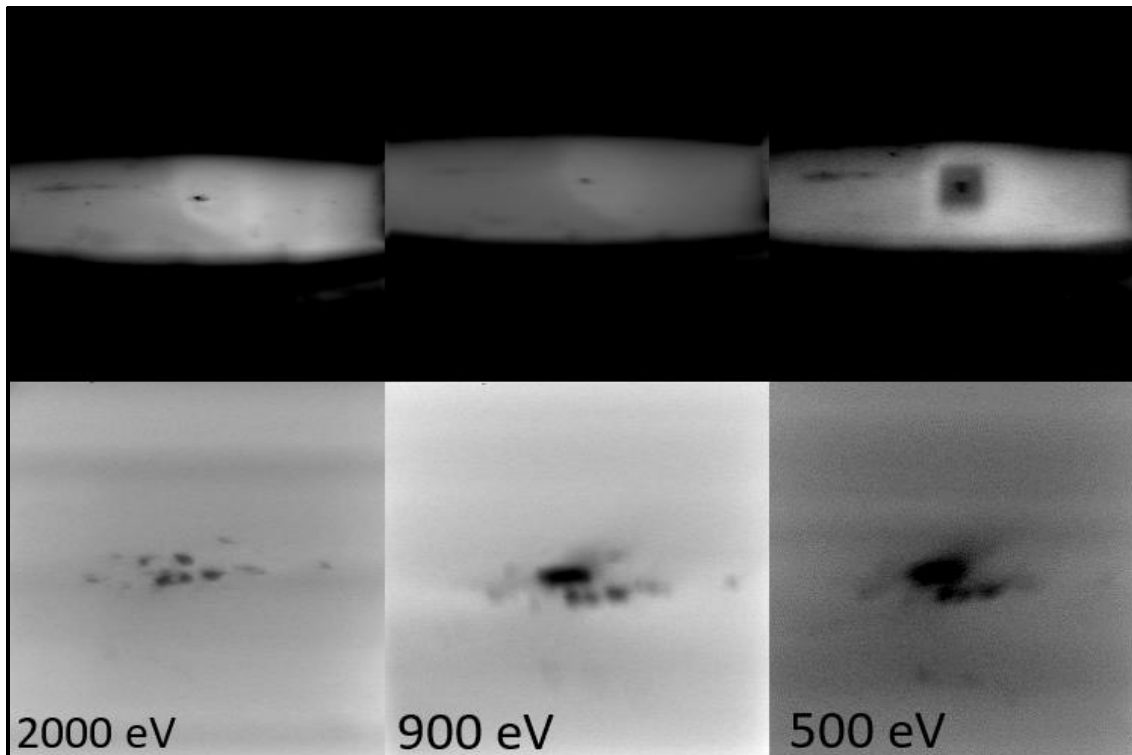

Figure 4: Above: Overview of typical NanoMill® images. Below: Recording of the same sample at three different acceleration voltages (2000, 900 and 500 eV) are shown. Ion-induced secondary electrons (SE) are detected by an Everhart-Thornley Detector. Less SE are produced at low acceleration voltages and that lead to blurry and noisier images.

The sample is tilted at +10° and the images were taken at an acceleration voltage of 500, 900 and 2000 eV. The lower the acceleration voltage, the worse the image quality. Consequently, due to the lower secondary electrons yield, the image is more blurred and noisy. At 2000 eV, single holes in the sample can be seen separately, while at 500 eV, it is difficult to identify individual holes. The vacuum system consists of a turbomolecular drag pump and a diaphragm pump, both oil-free. Those pumps produce a vacuum of $2.25*10^{-7}$ torr in the main chamber. The load lock is used to insert the sample into the vacuum chamber of the NanoMill®. A gate valve separates the main vacuum chamber from the pre-vacuum chamber, so it is not necessary to vent the main chamber. Thanks to this it is possible to work immediately after transferring the sample into the main vacuum chamber. To transfer the sample to the holder into the sample stage, a transfer rod is needed. The sample stage permits a 360° rotation of the holder and the sample can be tilted in the range of -10° to +30°. If the sample is temperature sensitive, cooling the stage with liquid nitrogen down to -160°C is possible but in this master thesis all experiments were performed at room temperature. [6]

To summarise, this technique allows polishing the surface and thinning the sample over a longer milling time, while largely avoiding artefacts introduced at higher voltages, as with the PIPS™ instrument.

2.2 Microscopy Methods

2.2.1 Visible Light Microscopy

There are two different types of microscopes used in this thesis: the visible light microscope (LIMI), which is described in this chapter, and the transmission electron microscope, Philips CM20 (see section *2.2.2*).

For image correlation throughout varying magnifications available in LIMI and the TEM (comparison of the NanoMill® image with light microscopy image, see *section 4*), a Zeiss Axioplan light microscope, which can be seen in *Figure 5,* is used in transmitted and reflected mode.

The most important parts of the light microscope are:

- Digital camera
- Ocular
- Objective lenses
- Sample stage
- Condenser lens
- Illuminating device
- Focus adjustment

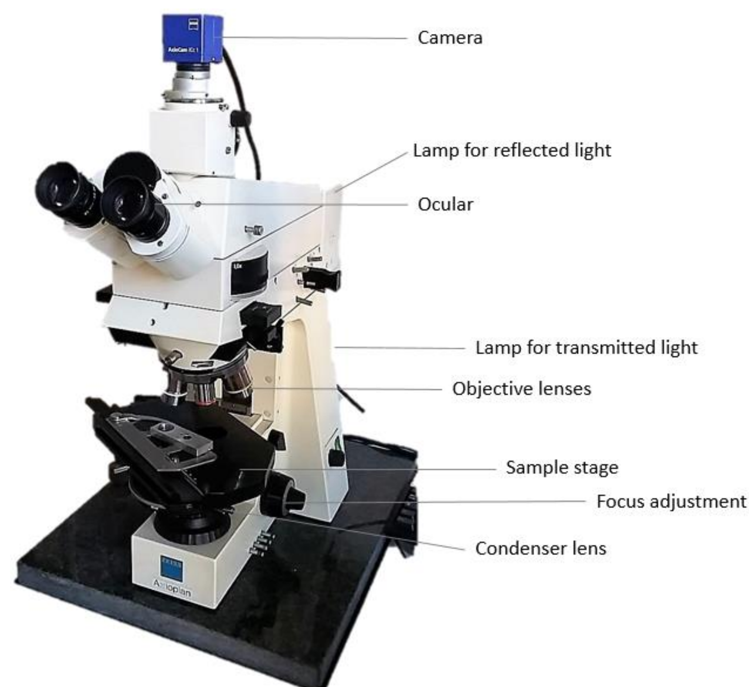

Figure 5: Zeiss Axioplan used for LIMI images, labelled with the most important parts.

There are two possibilities to illuminate the sample using either bottom transmitted light or upper incident light. In the transmission mode, the light comes from the bottom and passes through the sample before collection by the objective. The incident light either passes the objective before illuminating the sample or approaches from the side. With this technique, it is also possible to analyse opaque and thick samples. [18], [19]

2.2.2 Transmission Electron Microscopy

This chapter gives a short introduction to fundamentals of transmission electron microscopy. In addition, an established method to determine the relative thickness of a TEM sample in EFTEM mode– the "t/λ"- method – is introduced. In this thesis, it is applied to study thickness changes of the thinning process.
The setup of a TEM is remarkably similar to that of a LIMI. The TEM operates on the same basic principle but uses electrons instead of light. A Philips CM20 200 kV transmission electron microscope was used for TEM analysis in this thesis.

Figure 6 sketches the components of a TEM. It consists of three main stages:

(1) an electron beam producing cathode and beam shaping lens system (electron gun, condenser lenses)

(2) the goniometer with the sample and an imaging stage (sample, objective lens, projector lenses)

(3) an image recording system (fluorescent screen, digital CCD camera) and various apertures (condenser, objective, selected area electron diffraction)

Furthermore, the TEM requires a vacuum system with several pumps, working at different pressure levels, pressure gauges and a power supply.

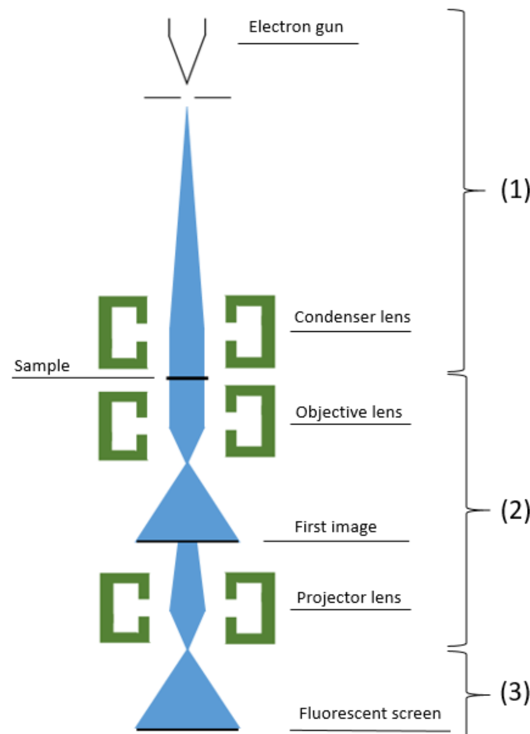

Figure 6: Schematic image of the TEM components with (1) electron beam producing system, (2) image producing system and (3) image recording system.

An electron gun, located at the top of the TEM, emits electrons that are accelerated with a high voltage, in our case at 200 keV. The condenser lenses typically form a parallel illuminating beam (if not used in a convergent beam mode). The electron beam passes the thin sample, experiencing scattering events, and enters the objective lens, where an image is formed (in addition to a diffraction pattern in its back focal plane). The following projector lenses enlarge either the image (or diffraction plane) and hence control the magnification. The level of detail in the image is described by the resolution of the instrument and is ultimately determined by the wavelength of the radiation and the quality of the lenses. Resolution is the smallest distance between two objects that can still be separated. Resolution (δ) depends on the wavelength (λ) and can be expressed by the Raleigh-criterion (1). In this equation, λ is the wavelength of the radiation (electron); μ is the refractive index of the medium and β the semi-angle of collection. Consequently, since the wavelengths used in light microscopy (380 – 800 nm) are much longer compared to accelerated electrons (2,51 pm @ 200 kV), electron microscopy is far more powerful in terms of resolution than LIMI and can reach atomic lengthscales. [2], [20]

$$\delta = \frac{0.61\,\lambda}{\mu\,\sin\beta} \tag{1}$$

λ … wavelength of the radiation
μ … refractive index
β … half angle of collection

The imaging principles in TEM rely on the scattering interactions of electrons with the thin sample. Elastic or inelastic scattering of the incident electrons generate several signals, such as secondary electrons and X-rays. This can be seen in *Figure 7.* [1], [2]

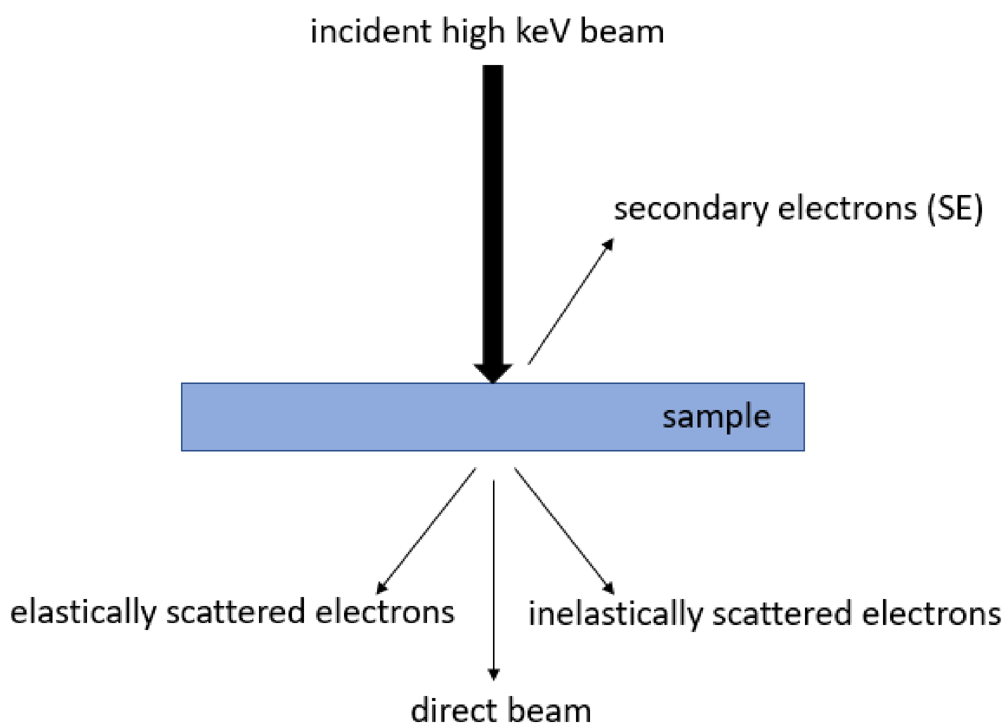

Figure 7: Scheme illustrating the signals (relevant for this thesis), generated by the interaction of electrons with a sample.

The elastic and inelastic interactions from electrons with matter are used for the different methods in imaging and spectroscopy. In this master thesis, two techniques based on inelastically scattered electrons are used: Electron energy loss spectroscopy (EELS) and energy-filtered transmission electron microscopy (EFTEM). For EELS, the energy losses of the incident electrons after inelastic scattering are analysed by an EEL spectrometer, whose key elements are an energy-dispersive prism, multipole lenses and a CCD camera, and then displayed in the form of spectral intensities [21].
Its imaging counterpart EFTEM allows the selection of electrons with specific energy losses by inserting a narrow, variable slit at the spectral plane. The following multipole lenses then form an energy-filtered image, or alternatively, the slit can be retracted to yield conventional, unfiltered bright-field (BF) images. EFTEM allows determining the relative thickness of the sample via t/λ maps. [2]
TEM imaging, in general, represents an efficient tool for the characterization of a wide range of materials at thicknesses below 100 nm with resolutions down to the atomic level. Sample thickness is a general limitation and allows imaging of only a small part (field of view) of the sample. One also has to keep in mind that TEM is of 2D projective nature, not able to resolve 3D information of a sample, for which electron tomography could be

used. Furthermore, for organic and biological samples the relatively high electron doses can be disadvantageous. [2]

2.2.3 Thickness Measurement – t/λ-Method

EFTEM processed images are containing information about the thickness of a sample. Therefore, in order to determine the sample thickness in an absolute or relative way, the application of special analysis techniques is necessary. One of the most commonly used methods is called "t/λ"- method. It gives relative thickness information based on the inelastic mean free path of the electron in the examined material. In this study, thickness changes between different thinning steps have been studied with this technique.[22]

The inelastic mean free path is defined as the average distance an electron travels in the sample before it gets scattered inelastically. Incident electrons are scattered inelastically more frequently when the materials features a small mean free path. In addition, the thickness of the sample affects the probability of inelastic scattering: the thicker the sample, the higher the inelastic intensities in the EELS spectrum. Poissonian statistics can be used to calculate the scattering probabilities of an electron through thickness. [8] The equations (2) and (3) show the n-fold scattering (**P_n**) and no scattering (**P_0**) probability. Equation (4) for the relative thickness t/λ can be derived from this distribution, and the value amounts to <1 for statistically "single scattering" samples. [22]

$$\mathbf{P_n} = \left(\frac{\mathbf{t}}{\boldsymbol{\lambda}}\right)^{\mathbf{n}} \frac{\mathbf{1}}{\mathbf{n!}} \mathbf{e}^{\left(-\frac{\mathbf{t}}{\boldsymbol{\lambda}}\right)} \tag{2}$$

$$\mathbf{P_0} = \mathbf{e}^{\left(-\frac{\mathbf{t}}{\boldsymbol{\lambda}}\right)} = \frac{\mathbf{I_0}}{\mathbf{I}} \tag{3}$$

$$\frac{\boldsymbol{t}}{\boldsymbol{\lambda}} = \boldsymbol{ln}\left(\frac{\boldsymbol{I}}{\boldsymbol{I_0}}\right) \tag{4}$$

t … sample thickness
λ … mean free path
n! …factorial of n with n = 0,1,2…
$\boldsymbol{I_0}$… integral under zero-loss peak / intensity of ZL filtered image
$\boldsymbol{I}$ … integral under total spectrum / intensity of an unfiltered image
e … Euler's number

To obtain t/λ, the measurement of the total electron intensity (I) and intensity of elastically scattered electrons (I_0) is obligatory. The image is taken from electrons, which interact elastically during their travel through the sample, and is the so-called zero-loss filtered image (ZL, I_0), originating from the integral of the zero-loss peak (ZLP, typically 10 eV wide slit) in the EEL-spectrum. Furthermore, to get all information that is needed for the t/λ method, an image gathering all electrons of the whole spectrum must be recorded (I), this image is called unfiltered, with the energy-selecting slit being removed. [7], [8]
For the calculation of the t/λ thickness map a software called Gatan Digital Micrograph is used. This program visualises and analyses the captured ZL and BF image. An example for a ZL and BF images as well as the resulting thickness map is shown in *Figure 8* and *Figure 9*.

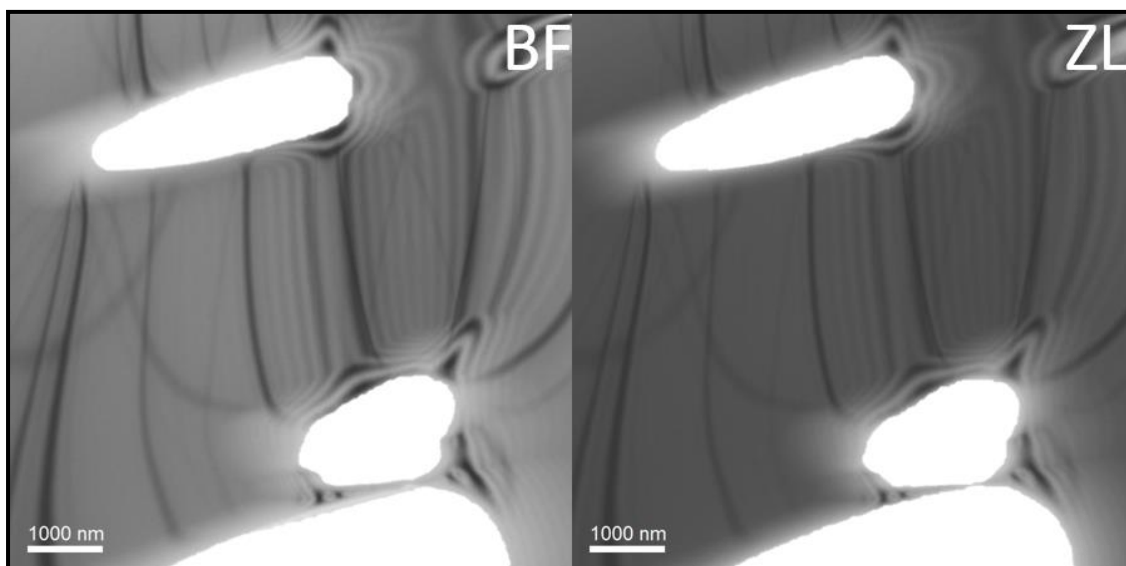

Figure 8: Unfiltered bright field (BF) image (left) and zero-loss (ZL) filtered image (right) of holes generated in silicon by ion milling with a PIPS™.

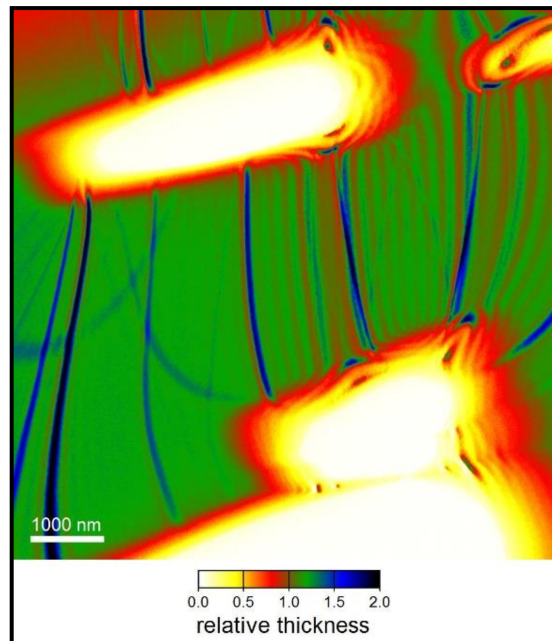

Figure 9: Relative thickness map calculated with equation (4) from figure 8, set to a contrast for t/λ between 0.0 – 2.0.

With Gatan Digital Micrograph the relative thickness map values can be colour-coded. This colouring technique enables a better recognition of the thinning process by making thickness differences visible, by setting the correct contrast limits.

2.3 Atomic Force Microscopy

Atomic force microscopy was used in the second part of the work to characterise the ion beam of the NanoMill®, by studying the impact shape on silicon, and to possibly get sputter rates.

The atomic force microscopy (AFM) technique makes it possible to acquire topography maps and other information at a resolution down to a few nanometers in lateral and sub-nanometre in vertical direction. The AFM can be used in environmental and in (ultra-) high vacuum conditions. Furthermore, the examination of the sample in a liquid environment and thereby, the analysis of in-situ processes is possible [23]–[25].

The main components of the atomic force microscope are a sharp tip at the bottom end of a cantilever, a piezo motion system, and a detection system. In *Figure 10* the setup of those components is shown.

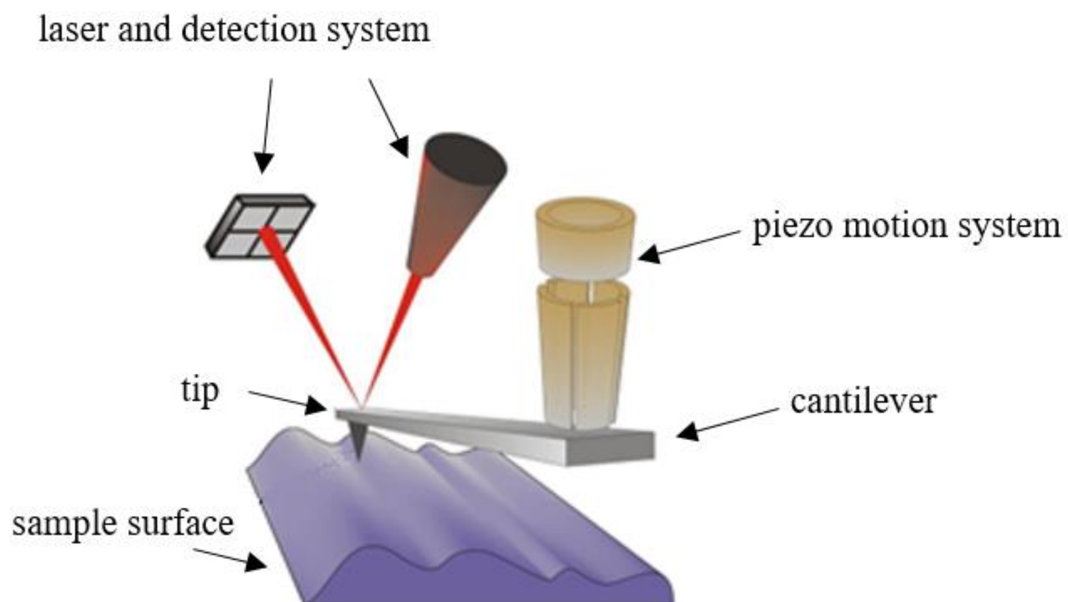

Figure 10: A schematic image of the AFM components: cantilever, tip, piezo motion system and laser detection system. [26]

The basic principle is as follows: A sharp tip is placed at the end of a cantilever. Attractive and repulsive forces have an effect on the tip when it approaches the surface. Those forces are bending the cantilever. Attractive forces between the surface and the tip cause the cantilever to deflect towards the surface (Van-der-Waals forces). If the tip touches the surface, the repulsive force (due to the Pauli-principle) takes over and the cantilever deflects away from the sample surface. Those forces are described by the Lennard-Jones

potential and can be seen in *Figure 11*. The bending of the cantilever is detected by a laser beam, which is reflected from the back of the cantilever onto a photodetector [26].

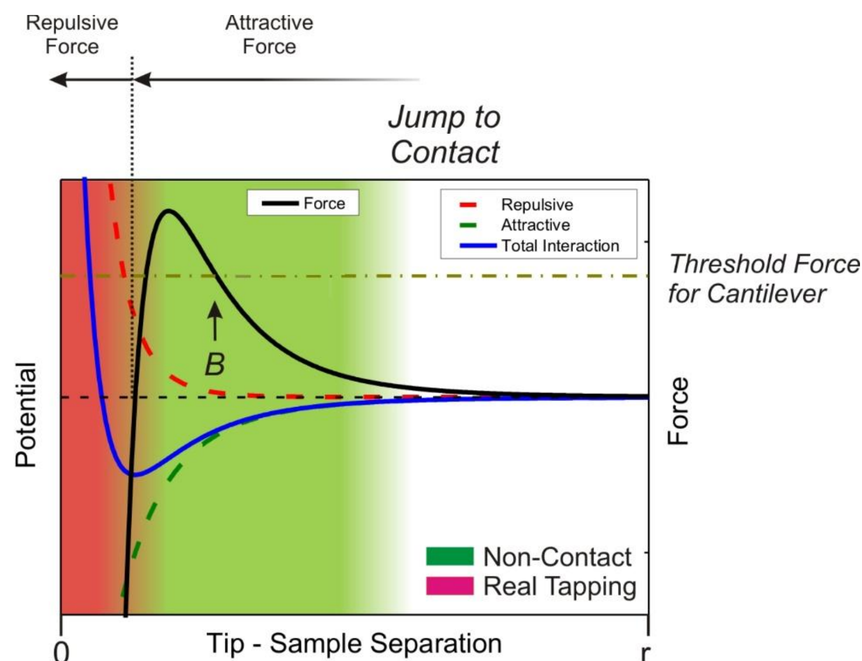

Figure 11: Attractive forces (green), repulsive forces (red) and resulting potential (blue, Lennard-Jones potential). The black curve shows the force on the tip. To the right of the black dashed line, the force is attractive and below it is repulsive. B marks the jump to contact distance. At the threshold force, the cantilever will snap towards the surface. In the tapping mode the tip switches between the red and green area. [26]

There are different operation modes such as tapping mode and contact mode. In this thesis, the tapping mode was used for measurements, where the cantilever is oscillating over the sample. A piezoelectric crystal stimulates this oscillation and the tip doesn't touch the surface permanently, it only taps at it periodically. This enables to examine sensitive materials thanks to a gentle treatment of the surface [26].

3 Practical Work

3.1 Sample Preparation - Overview

This chapter gives a general overview of the sample preparation methods used in this master thesis. *Figure 12* shows a flow chart of the preparation steps and visualises the procedure. All individual steps will be described in detail in the following sections.

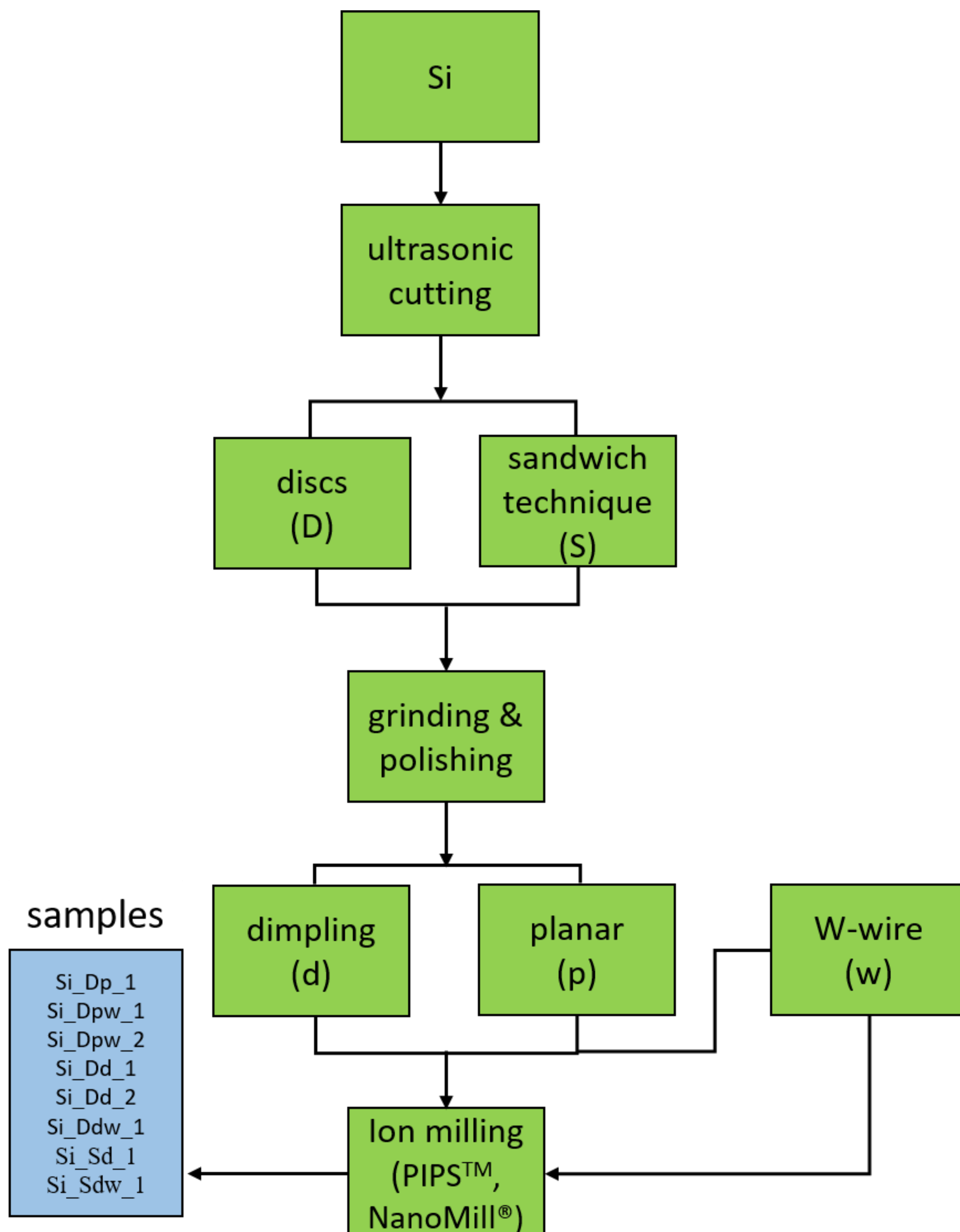

Figure 12: Overview of the sample preparation procedure. The letters in the round brackets are shortcuts for the techniques, which are used for sample naming. The produced samples are subsumed in the blue box.

In order to organise the samples as clearly as possible, a notation system was chosen for sample labelling that clearly reflects all essential preparation parameters (see *Figure 12*, the letters in the boxes). This notation is explained in more detail by an example, shown in *Figure 13*.

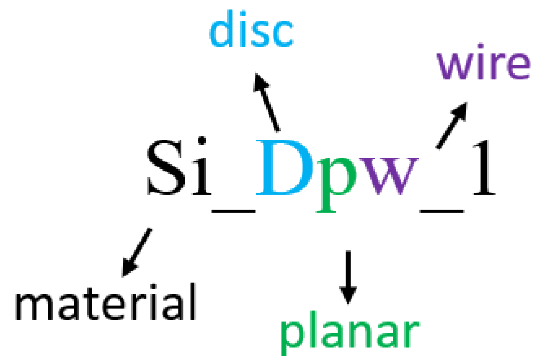

Figure 13: Description of the sample nomenclature: Si stands for the used material, D for disc preparation, p for the production of a planar sample, w indicates the wire marker method and the number at the end is the serial number.

The silicon wafer (Si) is first cut by ultrasonic cutting into discs (D) for the disc preparation technique [1] or into rectangles for further preparation using the sandwich cross-section technique [27] (S). All samples are then ground and polished to a certain thickness (100 µm for samples dimpled in the next step and 50 µm for planar samples). The preparation steps then split up into two possibilities: samples can be prepared planar (p) [28] or they can be thinned in the centre by a dimpling process (d) [1] Dimpled, planar and cross-section prepared samples are also used for a tungsten wire marker method (w). In the end, all samples are ion milled in the PIPS™ to electron transparency and post thinned and cleaned with low-energy ions in the NanoMill®.

3.2 Disc Preparation

To generate sample pieces, which fit into the TEM sample holder an Ultrasonic Cutter from Gatan [29] is used (*Figure 14, left*). [1], [14]

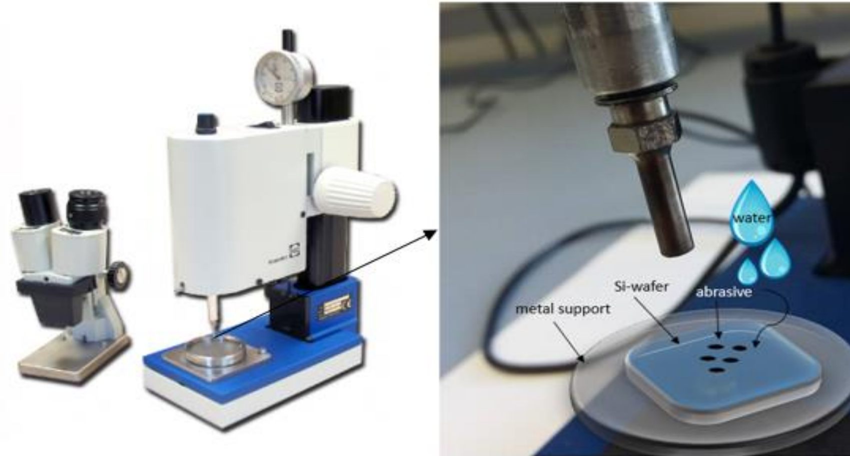

Figure 14: Ultrasonic cutter from Gatan (left) [32], components of the cutting (right): Si-wafer, abrasive grains and lubricant water.

At the free end of the instrument, it carries a toothless hollow cutting tool. The shape of the tool is circular in order to produce a disk with 3 mm in diameter. A silicon wafer piece is glued on a bulky, heavy magnetic metal support. This support is then placed on the machine platform under the hollow cutting tool, which is lowered until it touches the sample. Between sample and cutting tool, silicon carbide (SiC) particles as abrasive and water as lubricant are placed. (*Figure 14, right*). The abrasive is harder than the sample material and therefore, the grains produce friction and cut into the material. During cutting, a mechanical sensor constantly measures the progress of the cutting tool into the material [30].

To fix the sample parallel to the cutting tool, a spring-loaded platform helps to apply a constant force by pressing the sample up against the tool. It is important to keep the platform manually aligned with the sample so that parallel cutting is warranted. This technique can only be used for cutting bulk, thin film, single-phase or multiphase and brittle materials, and not for ductile, soft or very hard materials. A disc punch system is used for metals, alloys and ductile materials. [30]

After cutting out 3 mm discs, mechanical polishing is used to thin the samples and to produce smooth, scratch-free surfaces before ion milling. The matter is removed by abrasive particles, which are harder than the silicon disc. Before grinding and polishing, the initial thickness of the disc must be determined. The sample is glued on a cylindrical

support. For glueing, the cylinder is placed on a hotplate. After a few minutes, a small piece of wax is melted by touching the hot surface of the support. Then the sample is placed in the middle of the cylinder and gently pressed down with a tweezer. To cool down, the cylinder is removed from the hotplate. When the support cylinder has cooled down to room temperature, it is placed in the Disc Grinder. The Disc Grinder ensures stability and flatness of the sample during grinding. *Figure 15* shows the Disc Grinder and a cylinder with a Si sample, glued on top, as well as a Buehler Handimet Grinder (to fix the grinding strips) can be seen.

Figure 15: Buehler Handimet Grinder (left), Gatan Disc Grinder and support cylinder with sample (right).

With the micrometer screw on the Disc Grinder, the thickness, which is removed by grinding, is measured. It should be noted, that the glueing layer changes the initial thickness of the silicon wafer, so it is necessary to determine the thickness of the silicon disc and the glue. The simplest way is to measure the thickness of the disc, the cylinder and the cylinder-glue-disc combination. By subtracting the cylinder from the combination, one gets the thickness of disc and glue. With this information, the final thickness is ground in a controlled way as described below.

The grinding starts with a large grain size, which decreases with every grinding step. Grit sizes of 240, 320, 400 and 600 abrasive grinding strips (SiC sandpaper) are used for thinning the sample to approximately 100 µm, (for those are dimpled in the next step), or to 50 µm (for planar samples). Water is used as lubricant and coolant. Between the grinding steps, the sample must be checked under an optical microscope, to determine scratches or defects from the previous step. Different trajectories make it easier to distinguish scratches from the surface. A TexMet^{TM} polishing cloth is used. First, a 6 µm diamond suspension and water as lubricant are applied to polish the surface of the disc. For manual polishing, a rotary platform polisher is used. The final polishing step is

performed with a 0.25 µm diamond suspension. Before changing the grain size for the next grinding and polishing step the sample is cleaned with water and ethanol. The abrasive grains between the cylinder and the micrometric screw can be removed with a cotton swap. The cleaner the sample is, the fewer scratches caused by abrasive grains are found in the light microscope after every grinding step. A well-prepared, thin sample with a mirroring, scratch-free surface is the result of the mechanical polishing step.
The samples with a final thickness of 100 µm are dimpled in the next step. A Gatan Model 656-dimple grinder is used for dimpling (see *Figure 16*).

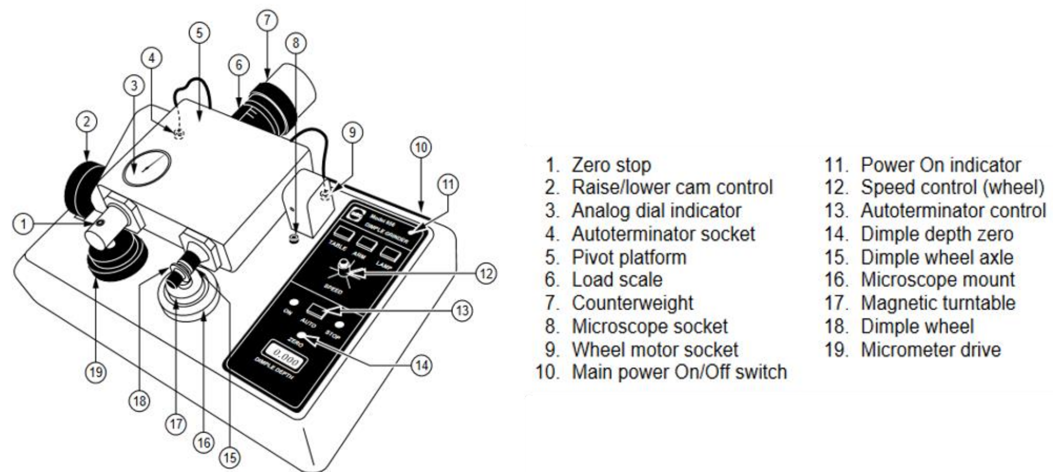

Figure 16: Components of a 656-dimple grinder by Gatan, which is used for thinning the sample in the middle. [31]

Dimpling is used to thin the centre of a 3 mm disc in diameter, or a cross-section with same dimensions, and about 100 µm thickness down to approximately 18 µm by grinding a spherical calotte. A greater edge thickness helps to prevent breakage of the sample while handling. Dimpling is also a polishing technique, which uses mechanical abrasion. [1], [31]
The sample is hot glued with the side to be protected to the centre of a support cylinder. The sample support is set onto an adjustable-speed vertical axle rotating stage (see character 17 in *Figure 16*). The grinding wheel (18) is lowered onto the sample mount near the sample and the counterweight (7) load of 20 g is set. Then the micrometer drive (19) is turned until the indicator needle (3) reaches zero. To set the zero point, the zero button (14) must be pressed. The sample is centred with a stereoscopic microscope. The desired dimple centre should rotate in the middle of the crosshair in the stereoscopic microscope. This is in particular necessary for cross-section samples, because there, their centre has to be at a glue line in order to get a hole there in the PIPS™ step. To set the final thickness, the micrometer drive has to be turned counter-clockwise until the display

shows the required thickness of 18 µm, but as a negative value. The arm, table motor and the auto-terminator are switched on. Finally, the grinding wheel is gently set on the sample with a small amount of diamond paste (grain size of 6 µm) as abrasive and a little bit of water as lubricant. When the desired dimple cavity thickness is reached, the auto-terminator stops grinding. Before polishing, the sample must be cleaned rigorously in order to remove any abrasive grains and to avoid scratches in the following step. For final polishing, the grinding wheel is replaced by a felt polishing wheel. First, the felt must be wetted with water and then, 0.25 µm diamond paste is set on the wheel. Before lowering the wheel on the sample, the arm and table motor are turned on. The sample is polished for about five minutes. Throughout this work, dimpling was done solely on one side of the sample. After this, the sample is thin enough for further thinning via other preparation techniques (PIPS™, NanoMill®). [31]

3.3 Sandwich Cross-section Preparation

With the sandwich technique, it is possible to analyse the cross-section of multilayer materials, to get information about the layer thickness, interfaces, composition gradient or the depth of implanted ions, particles etc. [1]

By ultrasonic cutting, which is described in *3.2*, four silicon rectangles with a dimension of 5x4 mm are cut out and cleaned with acetone and water. A two-component adhesive (Gatan G1) is used to glue the rectangles to a sandwich. The glue must fulfil several criteria: It must be resistant to the electron or ion beam and it must have a defined hardness. In common, the sample material is harder than the polymer and this can lead to abrasion of the glue during the preparation steps (grinding, polishing).[1]
Glue is spread in a thin film on the clean silicon surface and the rectangles are placed on top of each other. The surface of interest, which must be protected, faces the glue.

At the end, a Si/glue/Si-sandwich is formed. In *Figure 17*, a schematic sketch of the sandwich is shown.

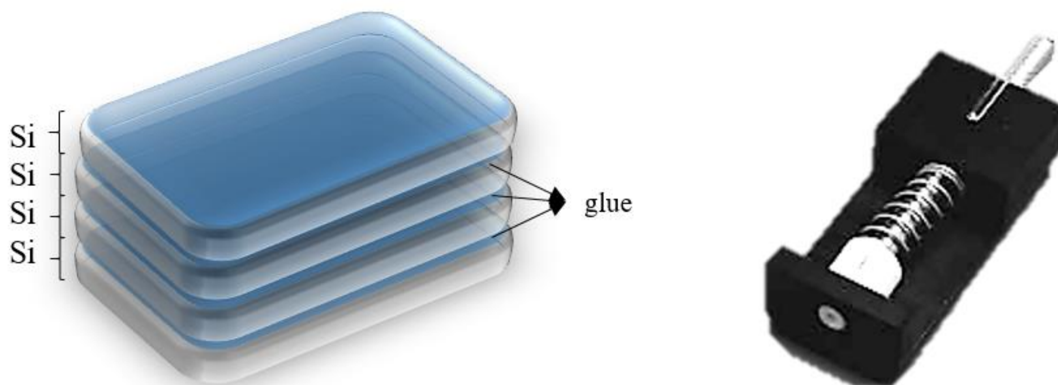

Figure 17: Schematic sketch of the sandwich layer structure (left), press for sandwich layer production (right).

A small press (see *Figure 17*, *right*) is used, to receive as little epoxy glue as possible between the layers. Teflon® helps to protect the sandwich from sticking to the press. The glue requires heat for polymerisation after sticking the silicon strips together. After two hours at 130°C in a low-temperature furnace, the curing process is finished. Next, a cylinder with a diameter of 2.3 mm is cut out of the sandwich with the ultrasonic disc cutter. For this, the sandwich is turned 90° and glued on a metal support again for stabilising the sandwich during cutting with the ultrasonic cutting tool (see section *3.2*).
The finished and shaped sandwich must be embedded in a metal cylinder for stabilisation. For this purpose, a brass hollow cylinder is placed on a Teflon® plate and filled with the two-component adhesive. Using a toothpick ensures that there are no air bubbles in the cylinder. The sandwich cylinder is placed in the brass cylinder and is cured for 2 hours at 130°C in the low-temperature furnace.
After the embedding process, the cylinder is cut into 500 µm slices with a wire saw. These cross-section samples can then be polished like the raw discs after the ultrasonic disc cutting. At the end, the samples should be approximately 100 µm thick and one side fine polished for the subsequent dimpling process.

3.4 Wire Marker Preparation

The objective of the wire marker preparation is to produce at a certain position two areas to analyse. Below is the description how the preparation is done.

On the flat side of a sample, a tungsten wire, having a diameter of 10 µm, is glued. A two-component epoxy glue (TC-EPO5-24), which cures within a few minutes, is used for glueing. First, the two glue components are mixed together. Very sharp tweezers are necessary to pick up the tungsten wire. While the glue gets more viscous, a piece of

tungsten wire of about 3 mm is cut and tipped with both ends into the glue. This should be done carefully so that only a little bit of the glue sticks to the wire ends. Under the light microscope, the wire is positioned on the sample that the glue sticks only at the outer edges of the sample. If dipping of the wire ends is done too early, the complete wire will be wetted with glue and will stick across the whole sample. This shall be avoided since the glue influences the thinning rate and quality. The mixing of the glue and sticking to the disc should not take more than five minutes. Otherwise, the glue is already too viscous. If the preparation went well – the wire sticks parallel to the disc and the glue is only on the wire at two spots at the sides of the sample – it can cure over night at room temperature.

3.5 Conventional Ion Milling with the PIPS™

The next point in the flow chart (see *Figure 12, page 19*) is the thinning process. In this section, the handling of the Precision Ion Polishing System (PIPS™) and the milling in the NanoMill® are described.

All samples are further thinned in the PIPS™ to electron transparency until visible holes are formed. First, the sample must be fixed in the sample holder. For this, a clamp-type holder (see *Figure 18*) is applied.

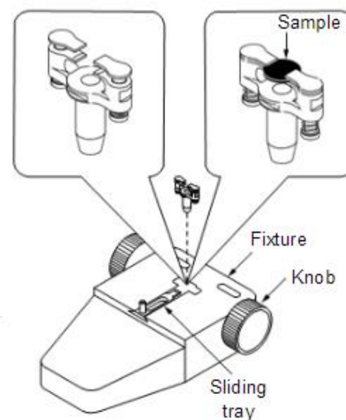

Figure 18: The sketch shows the clamp-type holder for fixing the sample and sample loading dock. [16]

The sample holder is put into the sample loading dock. By turning the knob counter-clockwise, the clamp opens. The mechanically prepared silicon disc is added on top of the sliding tray, which supports the disc, and it is pushed forward in between the open clamps. Now it is possible to align the sample between the clamps. If the sample has a dimple, this side must face downwards; thereby the observation with the digital camera (DIGICAM) is easier. The sample is fixed by turning the knob back. After attaching the sample, the sliding tray must be withdrawn. With a special tweezer, the sample holder is loaded into the airlock. Before loading, the piston must be raised. This is done by pressing the upper part of the airlock control switch. The sample mount rises from the working chamber into the airlock chamber. By pressing the "vent" button, the airlock cover can be removed and it is possible to load the sample. One has to ensure that the clamps are parallel to the notches, otherwise, the sample holder would be thinned too. After replacing the airlock cover, the "vac" button is pressed. By pressing the lower airlock control switch, the piston with the sample goes down into the working chamber. With the rotation speed control on the front, the desired rotation speed can be adjusted. The sample with the sample holder rotates counter-clockwise. The two ion guns are set to an angle of 6°

from below (due to the dimple on this side), 4° from above and the acceleration voltage is set to 4 keV. The observation of the sample and thinning progress can be controlled at any time easily with the camera. With a countdown interval, which has an alarm signal at its end, it is feasible to set a certain thinning time. There is a possibility to use an automatic shutdown, which works with a light sensor to stop the milling, as soon as holes have developed. When the sample thinning is finished, the unloading works exactly the other way around. [30], [15]

3.6 Low-Energy Ion Milling with the NanoMill®

After the conventional ion thinning step, all samples undergo a final thinning and cleaning process in the NanoMill® to reduce preparation-induced artefacts like amorphization and to reach the final thinness.

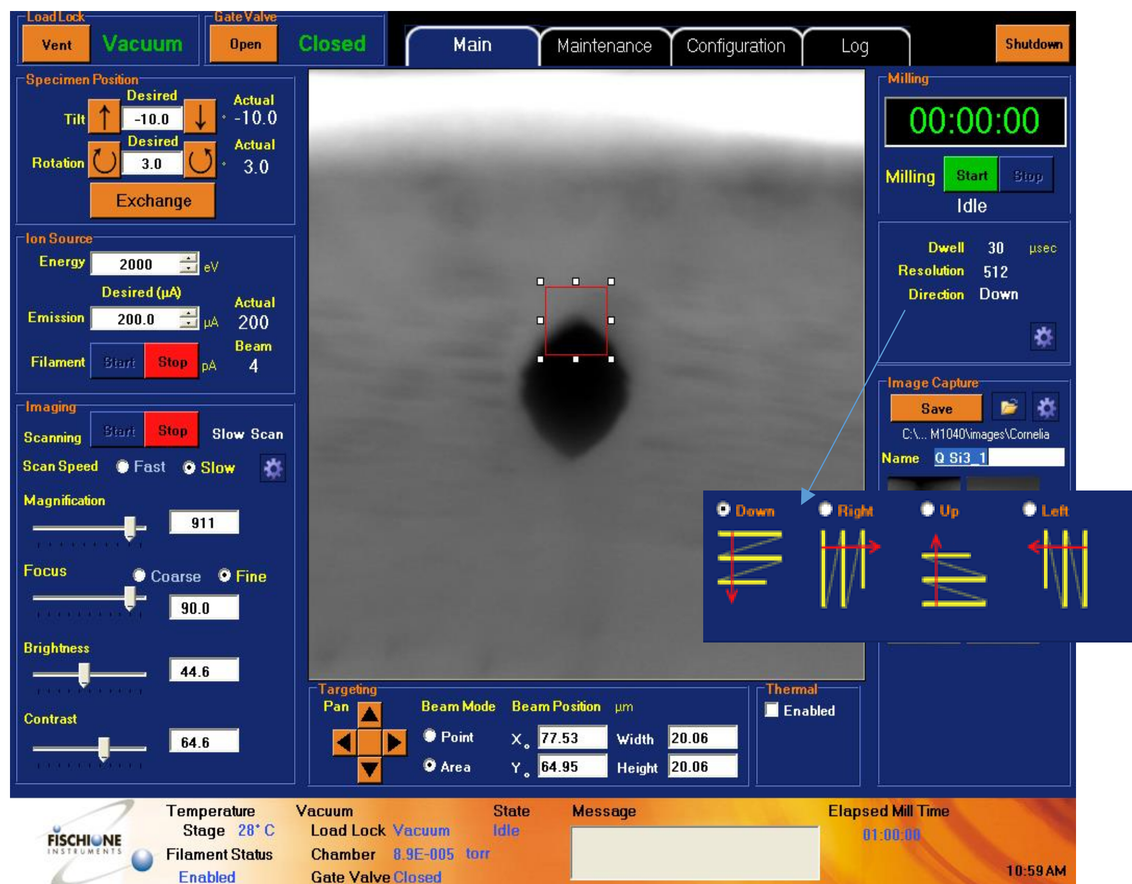

Figure 19: Operation interface of the software M1040 used for setting the milling parameters.

First, the sample must be fixed on a sample holder for which it is placed on a loading station. A screw needs to be loosened to open the clamp. The sample is placed and centred with the help of a stereoscopic microscope. The clamp attaches the sample at one side

when fixing the screw. If the sample has a dimple, this side faces down for a better visibility of the holes in the image.
For a safe transfer of the sample into the working chamber, a protective box is used. With the M1040 software (operation interface, *Figure 19*) the sample can be locked in at the vacuum chambers. The sample holder can be inserted by a transfer rod by venting the load lock. For this, the sample holder is screwed on the rod, the protective box is removed and after closing and pumping the chamber, the sample can be transferred into the main vacuum chamber and get its end position on the stage. Then, the rod is separated from the sample holder and pulled back. This step must be done very carefully because if the sample holder is not completely unscrewed from the transfer rod, it could happen that the sample holder falls into the vacuum chamber. Finally, the gate valve is closed and the necessary settings are done with the M1040 software at the user interface (main view). With the load lock and gate valve buttons the sample load, as described above, can be done easily. To get a clear as possible view on the sample, focus, brightness and contrast can be adjusted in the imaging box. A clear image is necessary to identify the sample position. Furthermore, the target window must be set to the sample in a way, that the ions only impinge the sample at the required point. In addition, the scan direction of the ion beam can be chosen (down, right, up and left), which can be seen in *Figure 19*. It is recommendable to choose a milling direction, which ends in the vacuum to avoid redeposition on the sample. [6]
Another important point is the correction of astigmatism. This is done manually with two screws, being turned minimally. The misalignment of the source and focusing lens is noticeable by a distortion of the image in the live view. This movement has to be minimised by turning the screws while changing the focus.
In this thesis, all samples are treated with the same milling parameters for reproducibility. They are listed in *Table 1*.

Table 1: Used NanoMill® parameters

Milling Parameters	
Source Energy	2000 eV
Source Emission / Beam Current	200 µA / 100 pA
Tilt	± 10°
Magnification	911
Milling pattern	20x20 µm
Milling time per side	1 h

All samples are tilted to +10° and milled with these parameters for one hour over a 20x20 µm milling pattern. Afterwards, the same procedure is done at an angle of -10°. A larger milling area leads to a lower milling rate, which means that larger thinning areas need a longer milling time to get the same result as smaller areas.

4. Results

This chapter gives information about the combination of observation techniques and findings for each individual sample.

After the mechanical sample preparation, the samples are pre-thinned in the PIPS^{TM} and analysed in the TEM CM20 for the first time. Due to magnification limitations in the TEM (minimum magnification 1350x with the objective lens still on), it is not possible to generate an overview of the entire hole, only a small part could be recorded at a time, as shown in *Figure 20.*

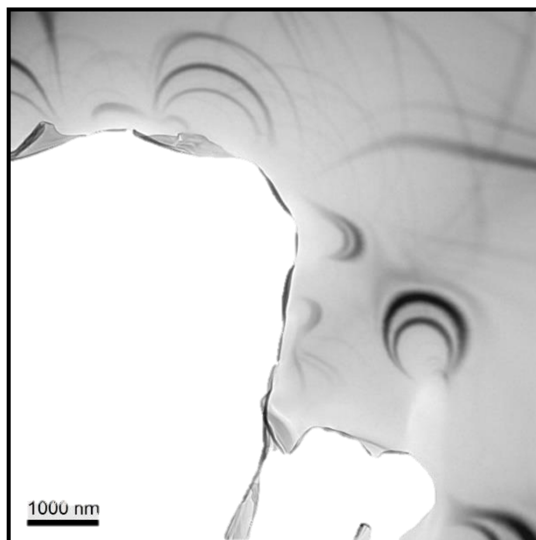

Figure 20: Example of a bright field image around a sample hole at a TEM magnification of 1350x, preventing a total overview of the entire hole.

As a solution, an image of the fluorescent screen is taken as an orientation guide to get an overview of the holes with the electron transparent regions at the edges. Subsequently, one significant hole is selected and t/λ maps (see section *2.2.3*) are produced to specify the relative thickness of the chosen area for further low-energy thinning. After TEM analysis, the sample is transferred back, and a SE image is observed at an acceleration voltage of 2000 eV, clearly revealing the holes. Unfortunately, just by comparing the fluorescent screen with the image at the NanoMill®, a precise relocation of the previously in the TEM selected and analysed sample area turned out to be complicated (see *Figure 21*).

Due to this, different observation techniques had to be correlated. The following section explains the considered workflow sequence, which is necessary to find and thin a certain sample position.

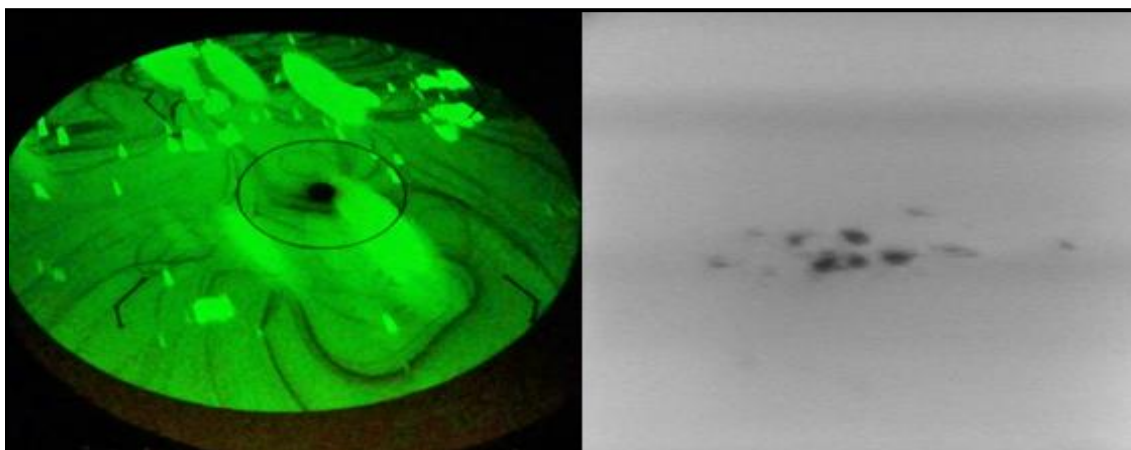

Figure 21: Photo of the TEM CM20 fluorescent screen (left) showing the holes, which are produced with the PIPS™; NanoMill® SE image of the holes in the sample (right). The TEM fluorescent screen by itself does not help to allocate the holes.

Thinking of a solution to get an overview of the whole milled area in order to receive a comparative image, the light microscope Zeiss Axioplan is used in reflected and transmitted mode at different magnifications to visualise this region. Since the sample is tilted by 10° during the thinning in the NanoMill®, which is leading to a distorted view of the sample surface – it is helpful to distort the LIMI image in a similar way to ease recognition of the selected area. The distortion is easily done in Microsoft® Office Word by pushing the image together lengthwise.

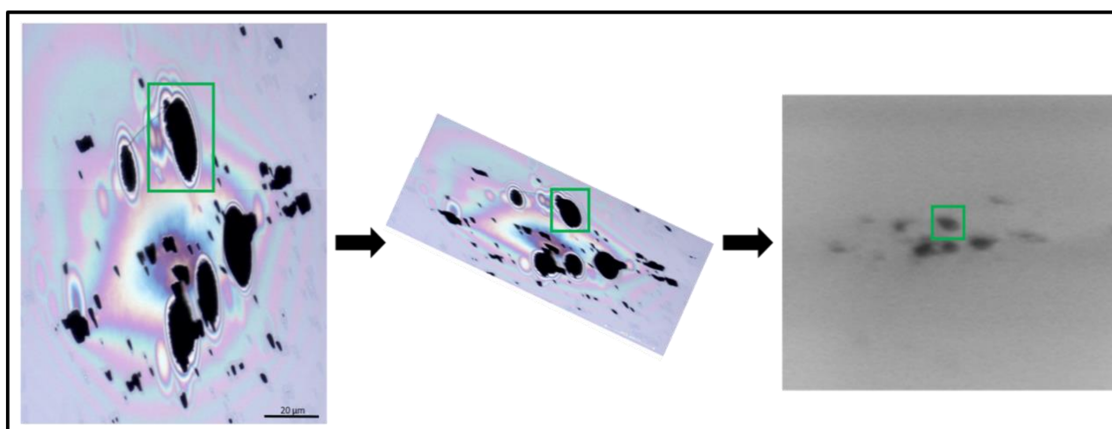

Figure 22: Optical distortion of the LIMI image (left) allows a better comparison of the images, and it is possible to rediscover the desired sample position at the NanoMill® (SE image right). By comparing the holes, visible in both images, recovery is feasible.

Now with this distorted LIMI image, it is possible to compare a certain hole position in all taken images (CM20 TEM fluorescent screen, LIMI and NanoMill® SE image), and to recover the chosen hole for further low voltage thinning. The procedure is summarised and visualised in *Figure 23*.

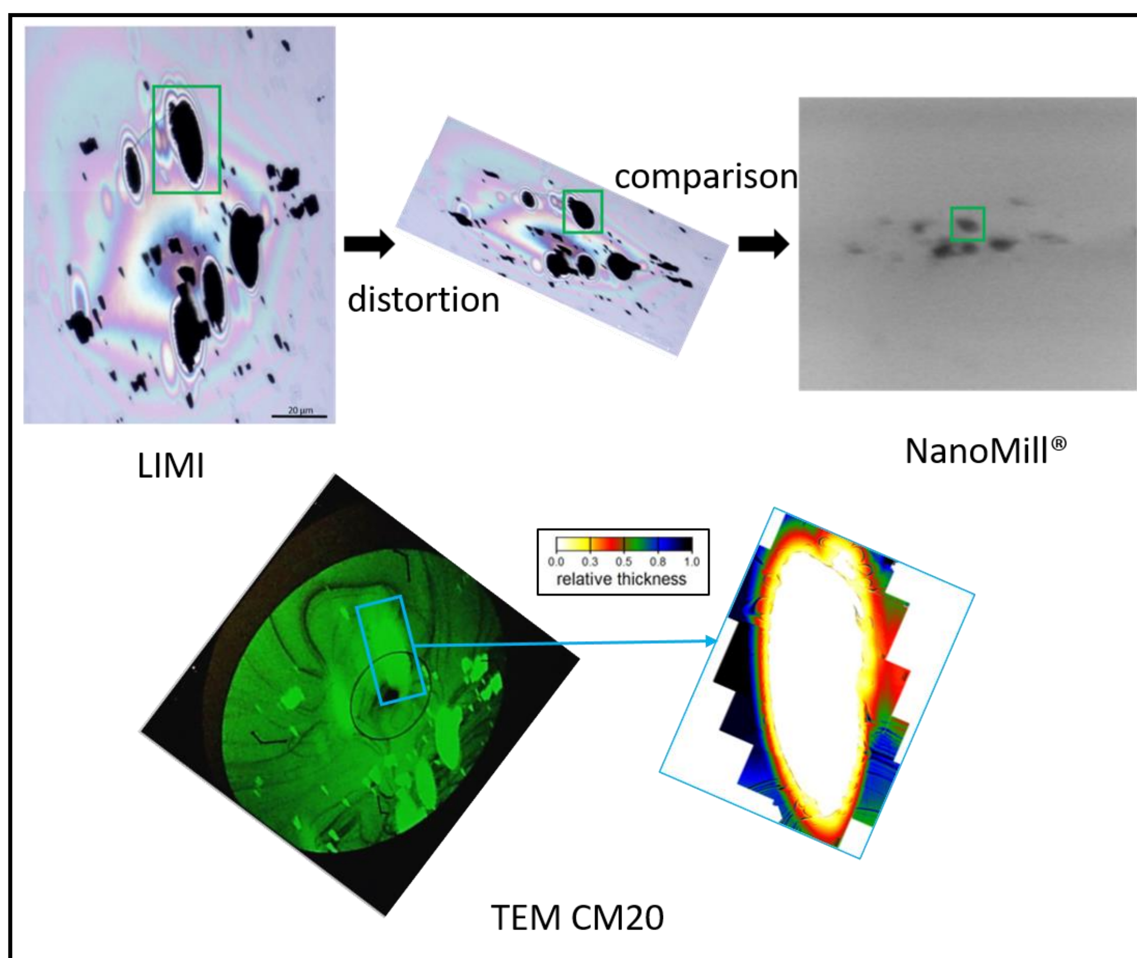

Figure 23: Pictorial summary of the working steps. Above: The LIMI images (original and distorted) are compared with the SE image from the NanoMill® Below: Same sample hole found with the help of the LIMI image and marked with the blue box in the fluorescent screen image and resulting relative thickness map.

After LE thinning, the sample is analysed a second time in the TEM and relative thickness maps are recorded to perceive if the correct position was thinned. As it turned out, the additional effort to take LIMI images is an important part of the recovery of the selected area and therefore, after the first sample investigation, an additional LIMI step was inserted into the workflow to be applied to all other samples. (*Figure 24*). Now, the LIMI images are taken after the PIPS^{TM} thinning and before the analysis in the TEM to generate an image comparable with the CM20 fluorescent screen so it is possible to choose an area for relative thickness measurements and further NanoMill® thinning of the same sample area.

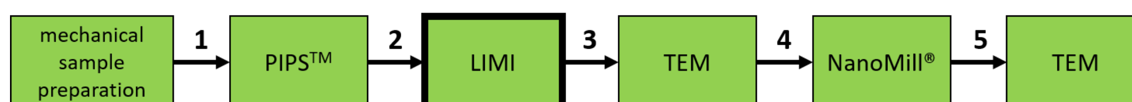

Figure 24: Optimised workflow after the analysis of the first sample. Due to the helpful LIMI image, they are taken before the analysis with the TEM to get an overview of the hole and to have a comparative image used at the TEM CM20 and NanoMill®.

Practically, quite often there is the need that a TEM sample is post-milled. This is because it is either too thick or the area of interest is not artefact-free for detailed TEM analyses and hence shall undergo additional thinning or cleaning with low-energy ions. Based on the workflow above, the beneficial LIMI step is performed after the first TEM examination (illustrated in *Figure 25*) so that a comparative image is available for NanoMill® thinning.

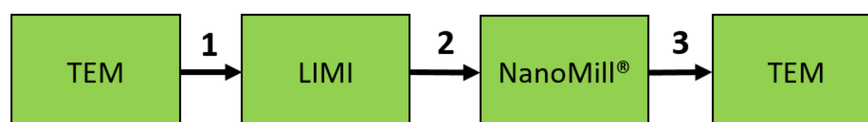

Figure 25: Potential workflow sequence, where the LIMI image is recorded after the first analysis with the TEM if a NanoMill® thinning is required.

The working process in *Figure 24* is used for all samples in this thesis. As a reference material, silicon is used. *Table 2* gives an overview of the prepared samples and includes sample geometry, thickness, PIPS™ parameters, and the NanoMill® thinning time. A detailed description of the individual sample results is given on the following pages.

Table 2: Overview of all prepared samples containing geometry, thickness, used PIPS™ parameters and NanoMill® milling time

	Sample	Si_Dp_1	Si_Dpw_1	Si_Dpw_2	Si_Dd_1	Si_Dd_2	Si_Ddw_1	Si_Sd_1	Si_Sdw_1
	Sample geometry	planar disc	planar disc	planar disc	disc with dimple	disc with dimple	disc with dimple	cross-section with dimple	cross-section with dimple
PIPS™	**Sample thickness (µm)**	53	70	60	96/18	98/18	97/18	100/18	100/18
	Rotation speed (rpm)	1	1	1	1	3	1	1	1
	Acceleration voltage (keV)	4	4	4	4	4	4	4	4
NanoMill®	**Milling time**	4 h 30 min	7 h	6 h 10 min	1 h 15 min	3 h 30 min	1 h 20 min	1 h 30 min	2 h

Sample: Si_Dp_1

Looking at the surface of the sample in *Figure 26*, one big hole is visible, which is surrounded by a few small holes. The whole surface is covered with shell-shaped ion induced thinning artefacts (marked with the blue circle). They occur because of the ionic bombardment of argon ions during thinning with higher energies in the PIPS^{TM}. [30]

The sample surface is not perfectly polished and shows fine scratches, thus, thinning started in an isotropic way along the scratches, labelled with the orange box in *Figure 26, A*. These affect the thinning time since the ion beam starts thinning in the scratches. The green square in *Figure 26, C* marks the sample position selected for NanoMill® thinning.

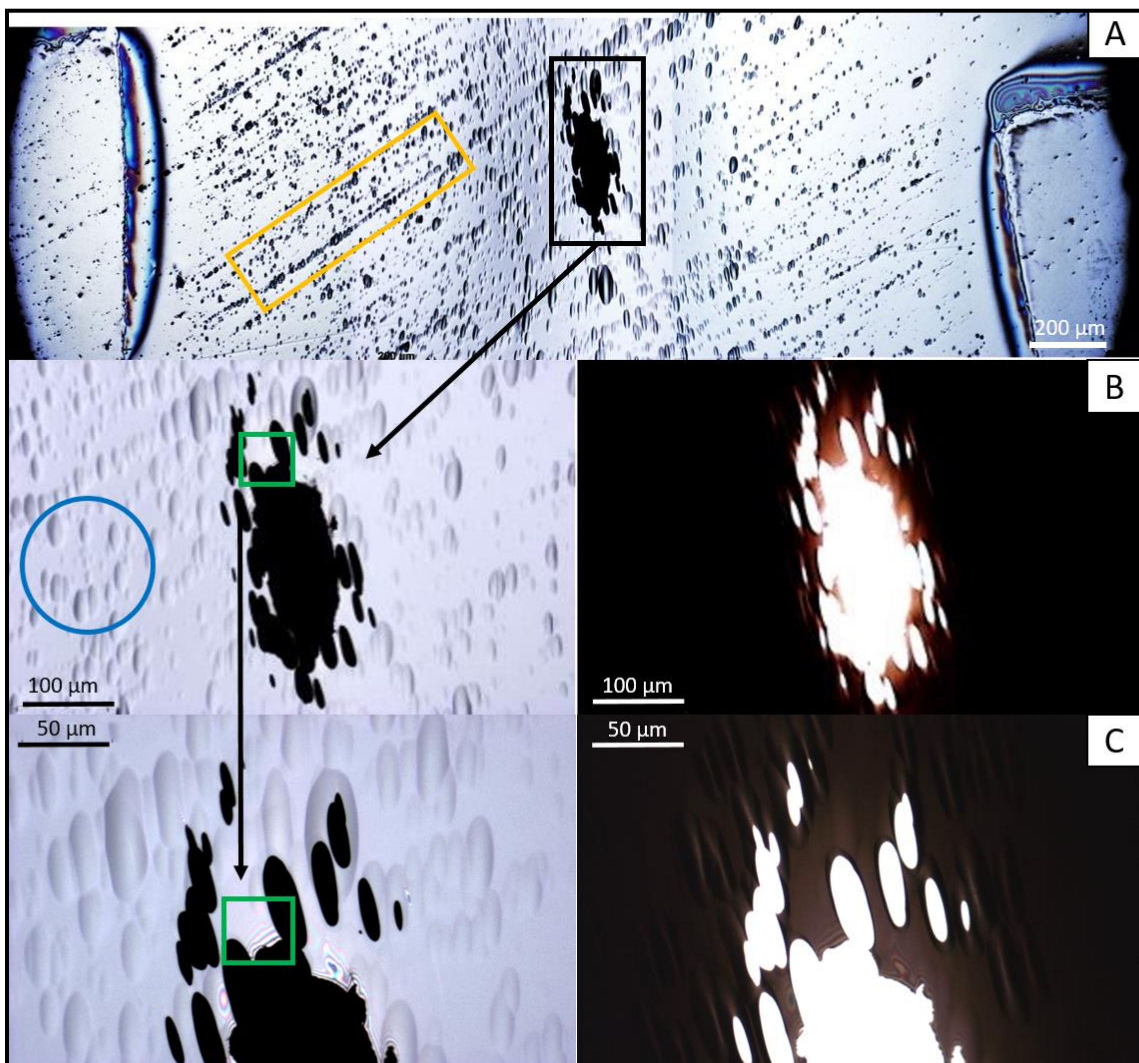

Figure 26: Light microscopy images of the Si_Dp_1 sample; A: overview, the orange box indicates the scratches, B and C: reflected light images (left) and transmitted light images (right) with a higher magnification where the blue circle labels the ion thinning artefact. The green box in C marks the position, which is thinned in the NanoMill® afterwards.

In *Figure 27*, a comparison of LIMI and the NanoMill® image is shown. The desired sample position can be determined with difficulties. It can only be found by means of optical distortion of the light microscopy image.

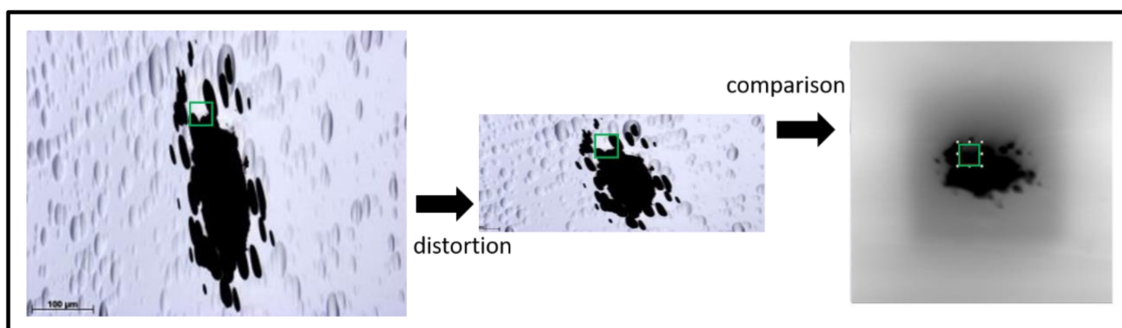

Figure 27: Comparison of the light microscopy image after distortion (left) with the NanoMill® image (right) of sample Si_Dp_1; the green box marks the sample position. The small holes around the big hole are significant features to find back the desired sample position for a subsequent NanoMill® thinning.

The relative thickness maps are composed of several single images, owed again to the fact of the rather high magnification on the TEM CM20. By comparing the resulting t/λ-maps in *Figure 28*, thinning can be monitored. Line profiles show a post-thinning factor of 1.4 (*Figure 28*, line profile). This thinning demonstrates the possibility to select a specific area for thinning and cleaning in the NanoMill®.

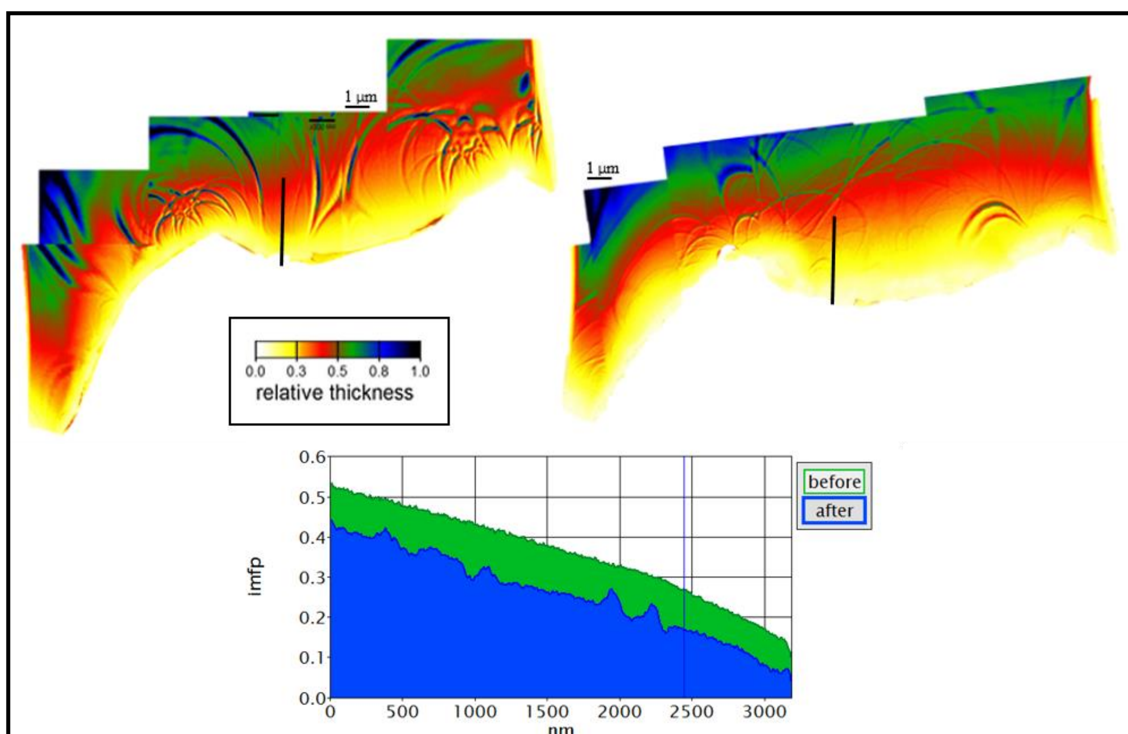

Figure 28: Si_Dp_1 relative thickness map t/λ of a certain sample position before (left) and after (right) additional milling with NanoMill®. The t/λ maps are merged to one picture. By comparing them with the help of line profiles, the thinning effect is visible and the post-thinning factor is 1.4.

Samples: Si_Dpw_1

The *Si_Dpw_1* sample is a planar disc with a 10 µm thick tungsten wire glued across the centre of the sample. The aim of the tungsten wire is the formation of holes at a certain position on the sample by serving as a barrier for the argon beam, where the beam cannot hit the surface. Two different areas for analysing on both sides of the wire are expected. The tungsten wire is fixed perpendicular to the clamps at the sample holder. After 1 hour 30 minutes thinning time, the wire vanished and no holes are formed. Afterwards, the sample is thinned until holes appeared to determine if the tungsten wire affected the sample thinning in any way. Only one area with holes is generated at a random area instead of two as expected (see *Figure 29*). Nevertheless, those holes can be used for further thinning steps.

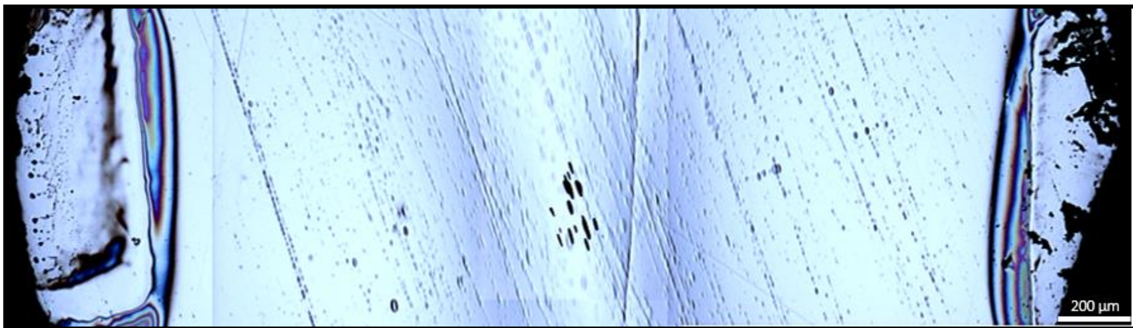

Figure 29: Overview of the light microscopy image of Si_Dpw_1 sample. The wire is fixed perpendicular to the clamps and vanished before holes are formed. Thinning till holes occurred led to holes at one position.

In view of this result, the wire position is checked with the help of the light microscopy image of the sample Si_Dpw_1. The distances from the wire position to the circle rim of the sample are marked with the red double arrows. Due to the difficult fixation, the wire is not exactly located in the centre of the sample (made visible with the red double arrows in *Figure 30*), but the holes are formed exactly in the middle (marked with green arrows).

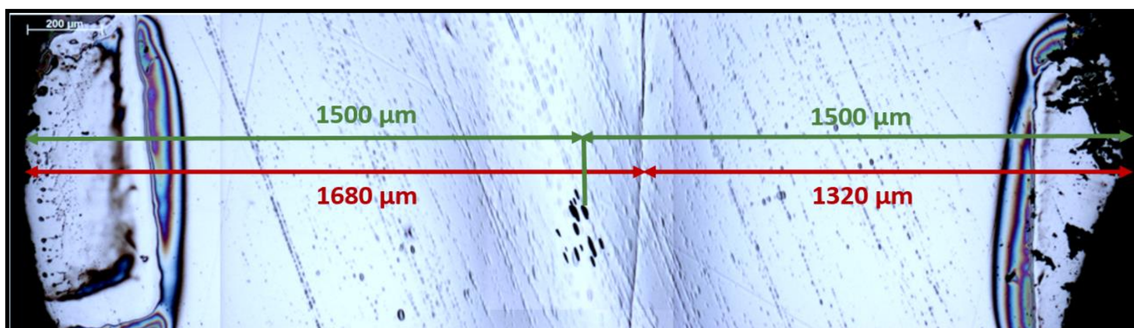

Figure 30: The red double arrows show the tungsten wire position and visualise, that the wire is not fixed exactly in the middle of the sample Si_Dpw_1. In addition, the holes are formed at the sample centre, optically visible with the green double arrows.

Sample: Si_Dpw_2

Sample *Si_Dpw_2* is prepared like *Si_Dpw_1* with the difference in mounting at the PIPS^{TM} thinning step, where the wire is fixed parallel to the clamps. This is done to check if the wire direction has an influence on the thinning result. The result of thinning sample Si_Dpw_2 can be seen in *Figure 31.* Like the samples before, the wire vanished before holes are formed and after thinning till they appeared, they occurred next to the wire at one position.

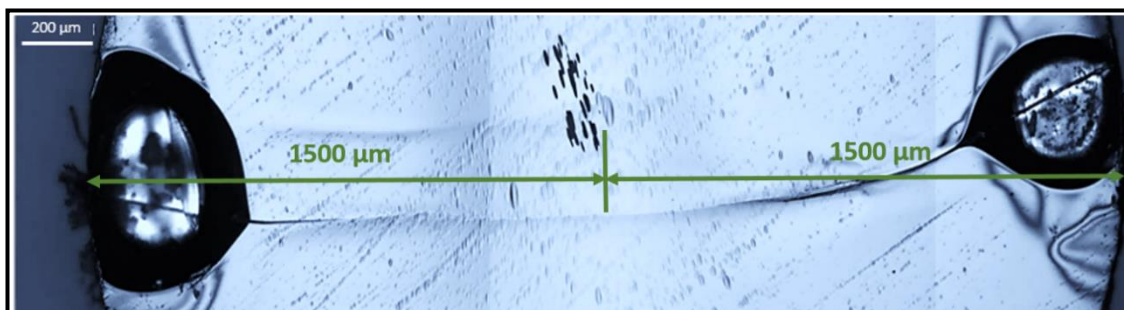

Figure 31: Overview of a LIMI image of the Si_Dpw_2 sample. The glue is visible on the left and right side. Holes are not exactly created in the centre of the sample, above the tungsten wire, which disappeared during thinning. The green double arrows mark the centre of the sample.

A LIMI image (see *Figure 32*) of the same sample is recorded 90° to the image taken before, to examine the wire position. The wire is not glued in the sample centre and additionally, the holes are not formed in the centre. For further analysis, it will be necessary to ensure, that the wire is fixed at the centre of the sample. Additionally, the sample should be thinner so that the wire remains longer on the surface.

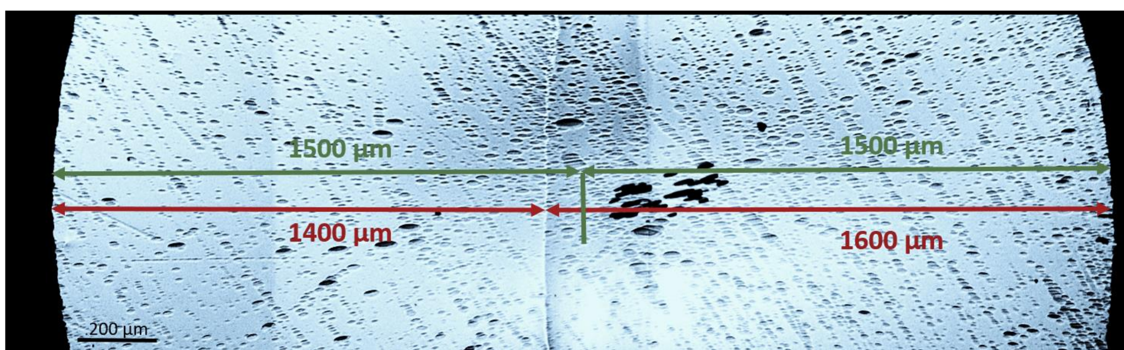

Figure 32: LIMI image of sample Si-Dpw_2, which shows, that the tungsten wire is on the left side of sample centre, instead of in the middle.

Sample: Si_Dd_1

Looking at *Figure 33*, many small holes instead of one big hole occurred at the dimpled centre during the PIPS™ thinning step. This took place because the sample is checked more often than the sample *Si_Dp_1,* where one big hole with small holes around occurred. Furthermore, less fine scratches and less shell-like structures are visible on the surface compared with the planar sample *Si_Dp_1*. The selected hole for further thinning is the hole, which is marked with the green box in *Figure 33*, C.

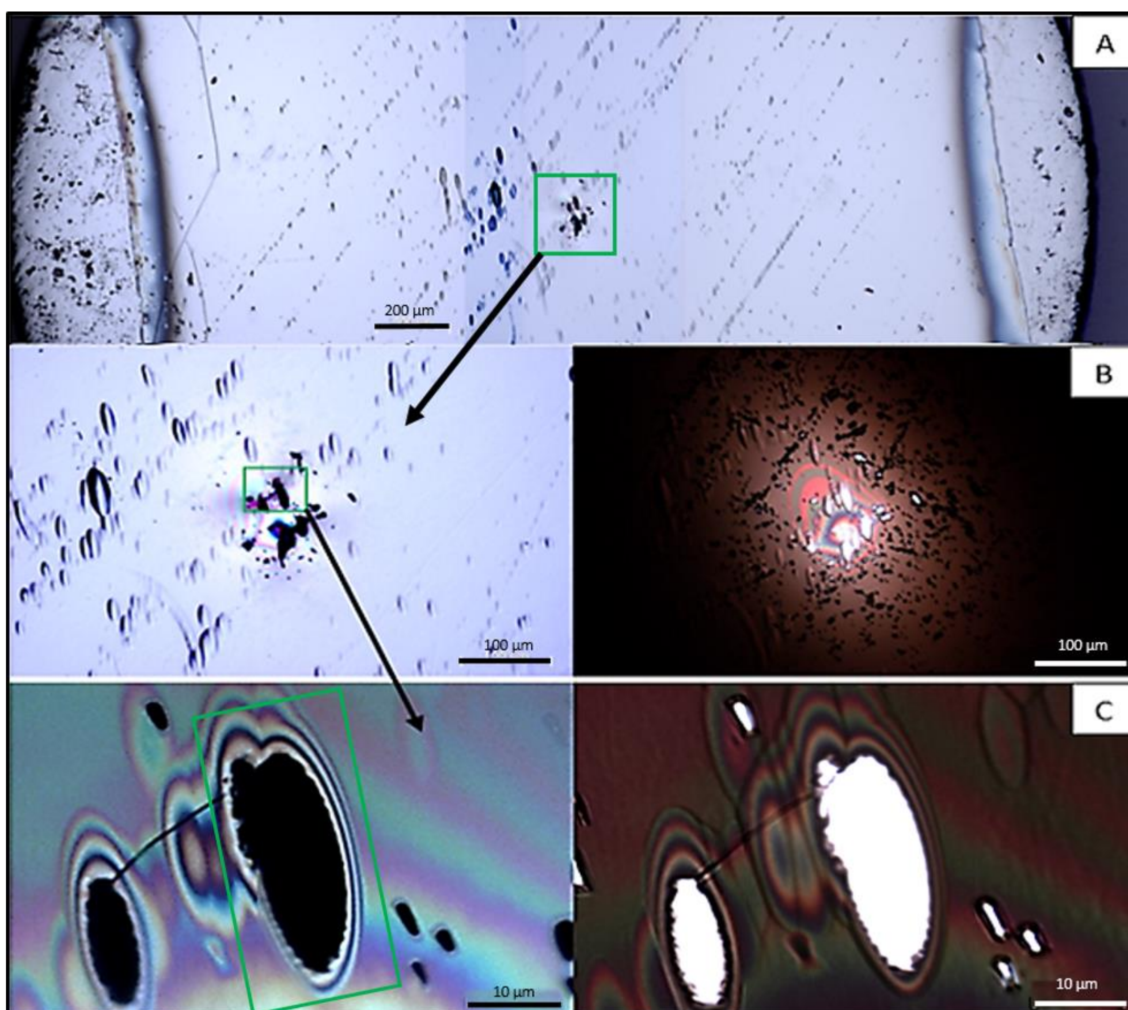

Figure 33: Light microscopy images of the Si_Dd_1 sample; A: sample overview; small holes are visible, B and C: reflected light (left) and transmitted light images (right) with higher magnification of the holes. The green box indicates the chosen sample position.

By comparing the LIMI image to the NanoMill® image, (*Figure 34*) the small holes can be assigned and the selected hole is found.

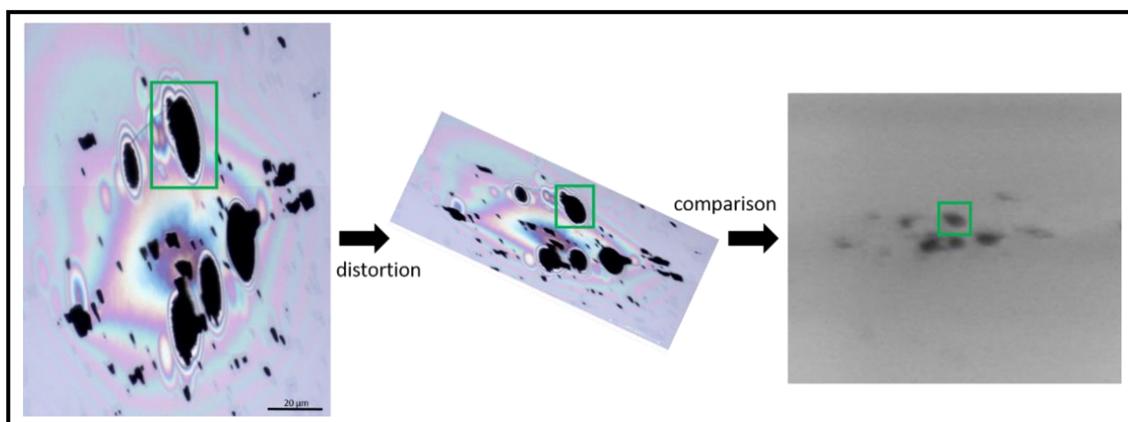

Figure 34: Distortion and comparison of the light microscopy image (left) with the NanoMill® image (right) of sample Si_Dd_1. This distortion helps to assign the holes at the NanoMill® image. The green box marks the selected and thinned hole position.

To determine, whether the selected hole has been thinned, TEM relative thickness measurements (see *section 2.2.3)* are done before and after the NanoMill® thinning step. The results of those images can be seen in *Figure 35* and thinning with a post-thinning factor of 2.86 can be observed.

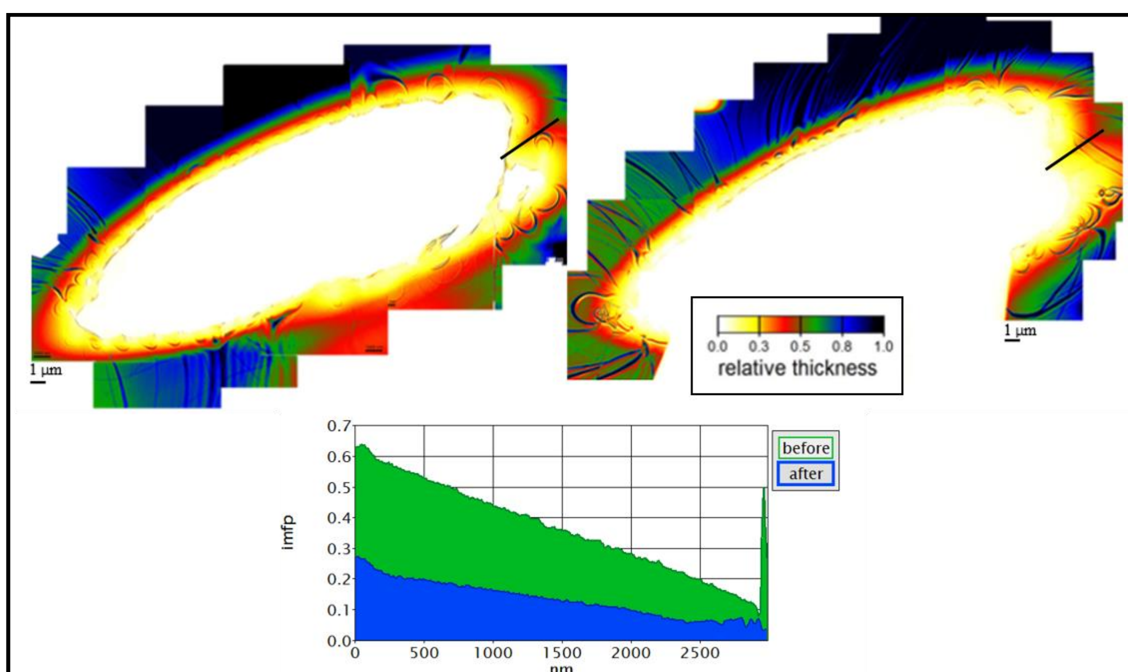

Figure 35: Si_Dd_1: Comparison of t/λ maps of the selected sample position before (left) and after (right) additional milling with the NanoMill®. Thinning with a post-thinning factor of 2.86 can be observed (down, line profile) around the hole and it can be recognised that a small part of the right sample got lost during handling.

Comparing the two images in *Figure 35*, the biggest difference is the missing part in the right image. By looking at *Figure 36*, a crack is visible. This part must have been dismantled during handling.

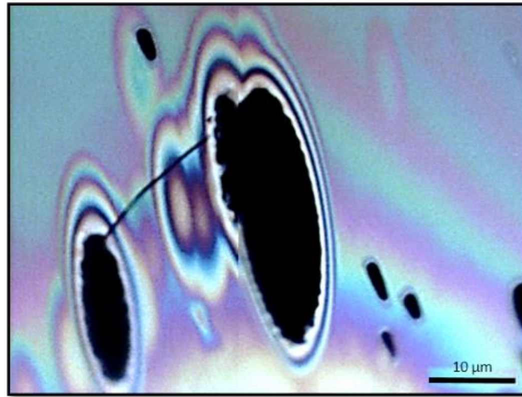

Figure 36: Crack, visible at the Si_Dd_1 sample.

Sample Si_Dd_2

Sample *Si_Dd_2* is prepared the same way as *Si_Dd_1*. Looking at the LIMI images in *Figure 37*, it is noticeable that there is one big hole surrounded by small holes like at sample Si_Dp_1. Furthermore, there is a star-shaped structure (indicated by the blue circle) observable, which is a mechanical preparation artefact. Diamond particles, which come from the polishing step, are located on the surface and a so-called curtaining effect occurs (formation of striations across the milling face). This effect results due to a change of the surface structure (diamond particles on a flat surface) and the different sputtering rates from silicon and diamond. However, the remaining polish on the surface does not have an effect on the milling result. [32]

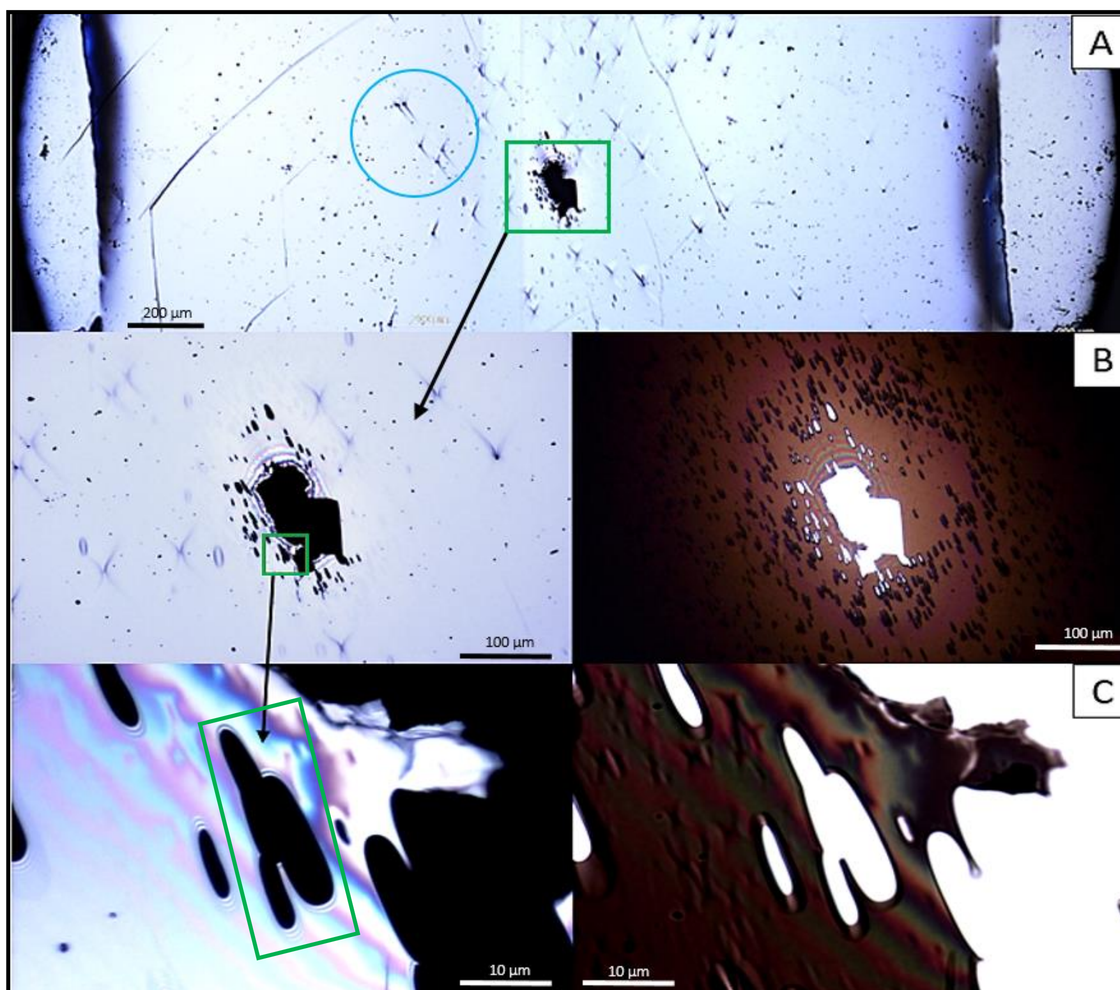

Figure 37: Light microscopy images of the Si_Dd_2 sample; A: overview, B and C: reflected light (left) and transmitted light images (right) with a higher magnification. A big hole with small holes around appeared. Star-shaped structures (blue circle) are visible, which are mechanical preparation artefacts. The green box marks the hole thinned in the NanoMill®.

By comparing LIMI with NanoMill® images (see *Figure 38*), the desired sample position can be determined, but it is much more difficult in comparison to Si_Dd_1 since the allocation of the holes is not as significant as at a sample with many small holes. A smaller hole near the big one is chosen for further analysis (see the green box in *Figure 37, C*).

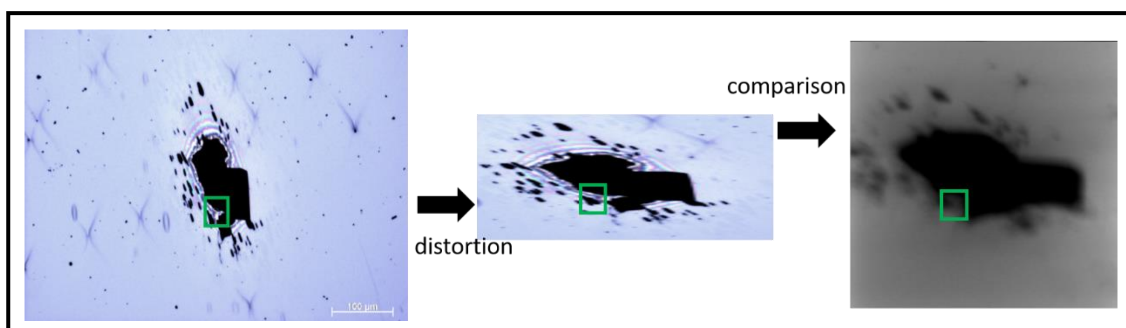

Figure 38: Comparison of the light microscopy image (left) with the NanoMill® image (right) of Si_Dd_2; the green box marks the selected hole for further NanoMill® treatment.

The small holes around the big hole are used to locate the chosen position. Using TEM relative thickness measurements and resulting t/λ maps (*Figure 39*) the thickness changes after the NanoMill® treatment are visible. Closer inspections show, that the hole is not thinned as a whole. This is attributable to this more difficult allocation and shows that the thinning window was not set exactly on the desired thinning position. The thinned area shows a post-thinning factor of 4.13.

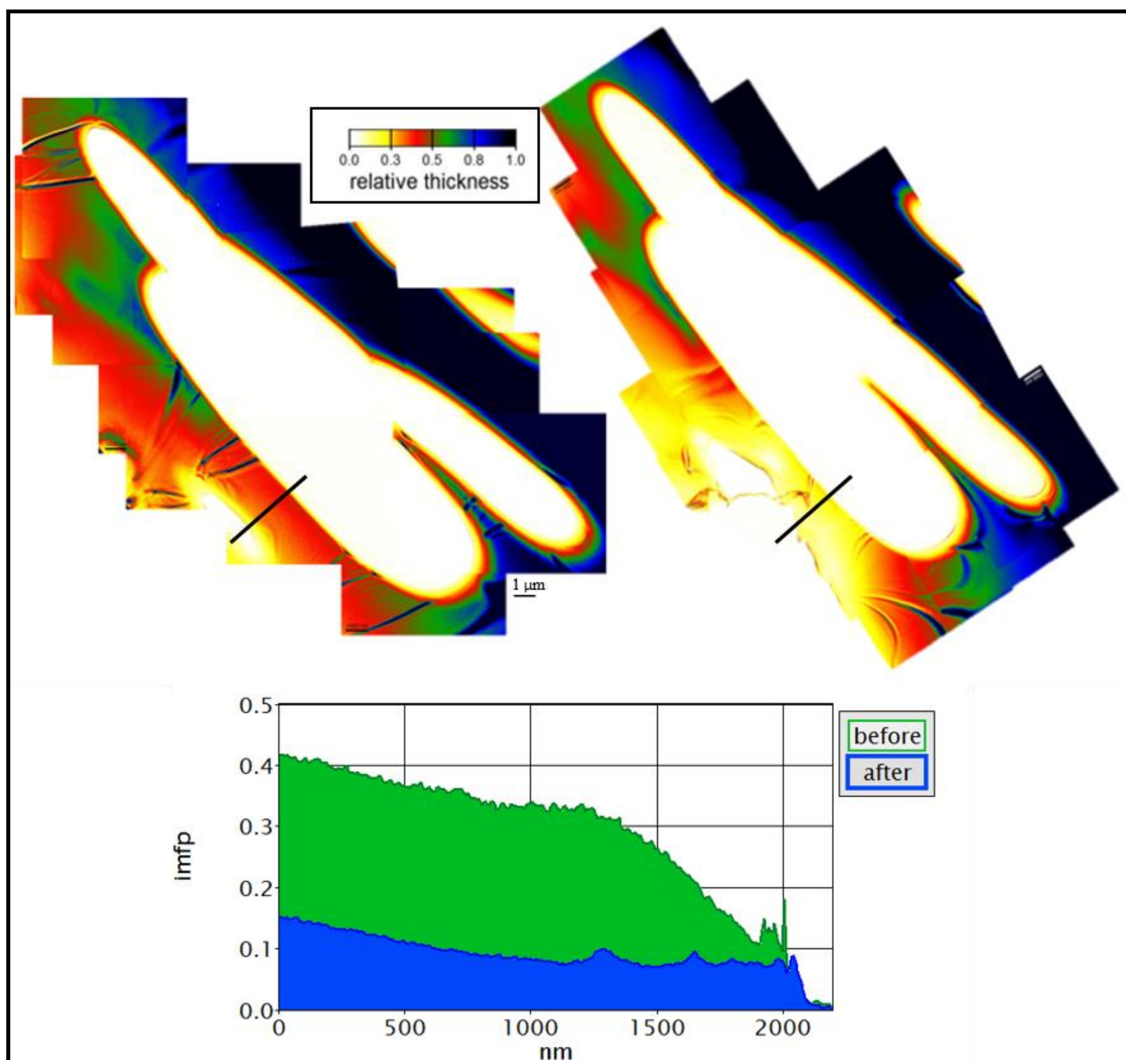

Figure 39: Si_Dd_2 t/λ map of a certain sample position before (left) and after (right) additional milling with NanoMill®. Thinning of the hole can be noticed but not the entire hole is thinned due to a wrong milling pattern position. A line profile is drawn at the thinned area, the post thinning factor is 4.13.

Sample Si_Ddw_1

This dimpled disc sample is used for the wire marker method, where the wire should still be at the sample by reason of a shorter milling time. The wire is glued on the flat side of the sample and is perpendicular clamped at the PIPS™ for the thinning step. As a result of a cleaner surface, no ion milling shell-like artefacts are visible, only a few star-shaped

structures are noticeable. Thus, cleaning the surface can lead to a near artefact free sample. As a result of thinning, one big hole appeared next to the wire after thinning. (see *Figure 40*).

Figure 40: Overview of a light microscopy image of the Si_Ddw_1 sample. A tungsten wire is glued perpendicular to the clamps at the PIPS™. Fewer artefacts are visible on the sample surface and one big hole appeared.

Similarly to sample Si_Dpw_1, the wire position is checked (*Figure 41*). The result is the same: The wire is not precise in the middle of the sample, where the thinned region (dimpled centre) is located. Unfortunately, the wire did not have any influence due to the wrong wire position. In order to ensure, that the wire is fixed in the middle of the sample, it is necessary to fix the tungsten wire directly at the LIMI in transmitted light mode because, in this mode, the thinnest sample region looks lighter than the surrounding thicker region.

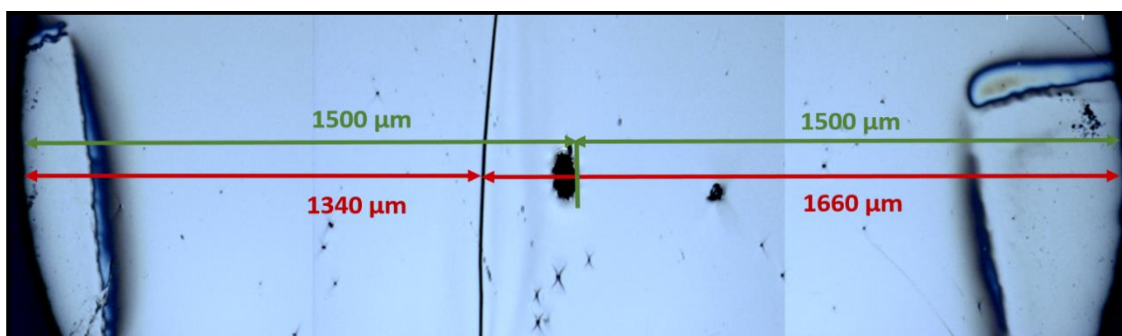

Figure 41: The tungsten wire position is determined and the red arrows show, that the wire is not in the middle of the sample. The green arrows confirm the differing position. At the sample centre, one big hole occurred.

The results of planar, dimpled and wire prepared disc samples can be summarised as follows:

Whether small holes or a big hole with small holes in the circumference appears is determined by the thinning time. At first, small holes are formed and after a few minutes, they merge to one big hole. In contrast to that, only a big hole is observed at planar samples and the PIPS™ thinning time takes three times longer than for dimpled samples.

If small holes are desired at planar samples, it is necessary to regularly check (for example every 10 minutes) the thinning progress. In addition, it has to be mentioned that the sample surface of planar samples showed much more milling artefacts due to the thickness, which can be seen in *Figure 42*.

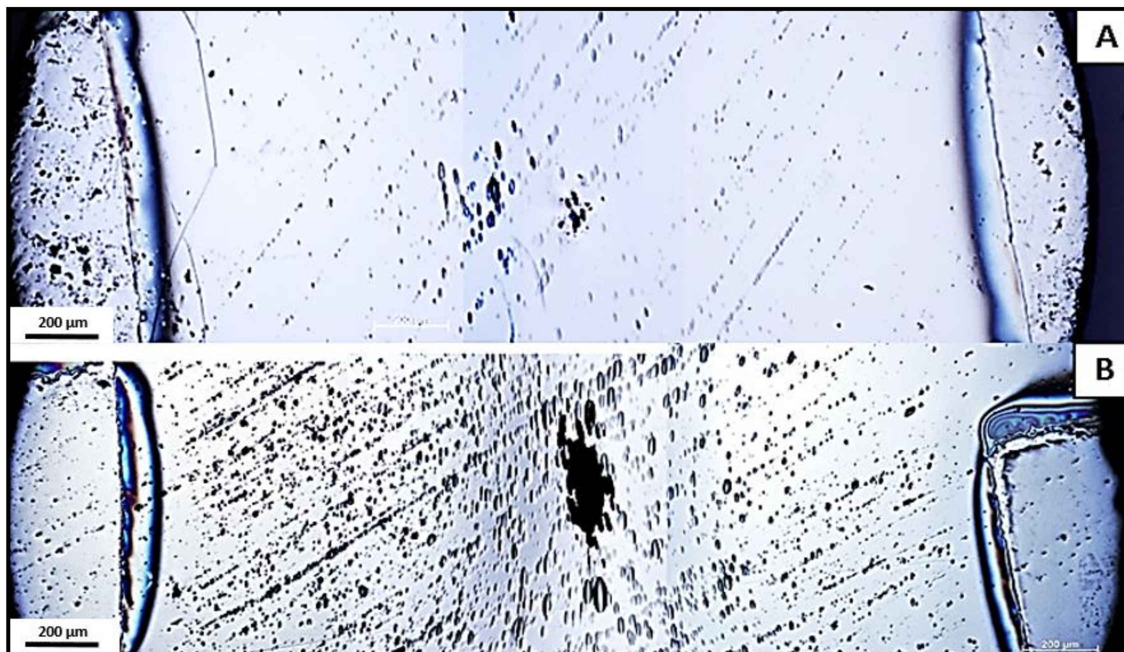

Figure 42: Comparison of the light microscopy sample overview of dimpled (A) and planar (B) samples. More milling artefacts are visible at the planar sample surface.

The following procedure would reduce the shell-structures on the surface: In the beginning, ion milling is done by higher incidence angles (> 10°) of the argon ions. When the sample gets thinner (the sample is brighter at the thinned region when switching it on), the beam angles are reduced (< 10°) for final milling until a hole appears. [30]

This leads to a smoother surface and a shorter milling time. An alternative way to get rid of the structures would be to produce thinner planar samples, for example by using the MultiPrep^{TM} system from Allied High Tech Products Inc. Samples of 20 µm thickness are produced easily with this technique. For the best thinning result, it is necessary to produce a sample free of scratches and as clean as possible.

The use of the tungsten wire method on planar and dimpled samples did not affect the sample thinning due to the wrong position of the wire on the sample surface. For dimpled samples, the use of the LIMI in transmitted light mode would help to fix the wire in the centre of the sample.

In order to be consistent in all experiments, and due to shorter thinning times and less milling artefacts, it was decided to use dimpled samples for the cross-section experiments.

Furthermore, many small holes are favoured, because they are more significant and the recovery of the sample position is easier for the following thinning step.

Sample Si_Sd_1

This sample is a cross-section prepared silicon sample with a dimple on one side. The sample has glue lines from the cross-sectional preparation, which are aligned and clamped parallel to the clamping (see *Figure 43*).

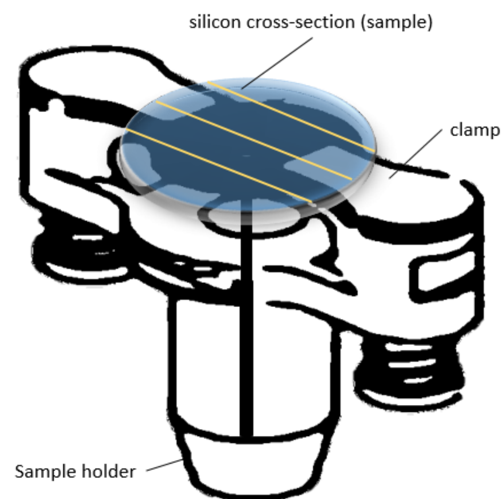

Figure 43: Illustration of the sample mounting direction: glue-lines parallel to the clamping. (modified from [15])

The image *Figure 44* shows, that the glue lines are visible on the surface. A long drawn-out symmetrical hole appeared during PIPS^{TM} thinning.

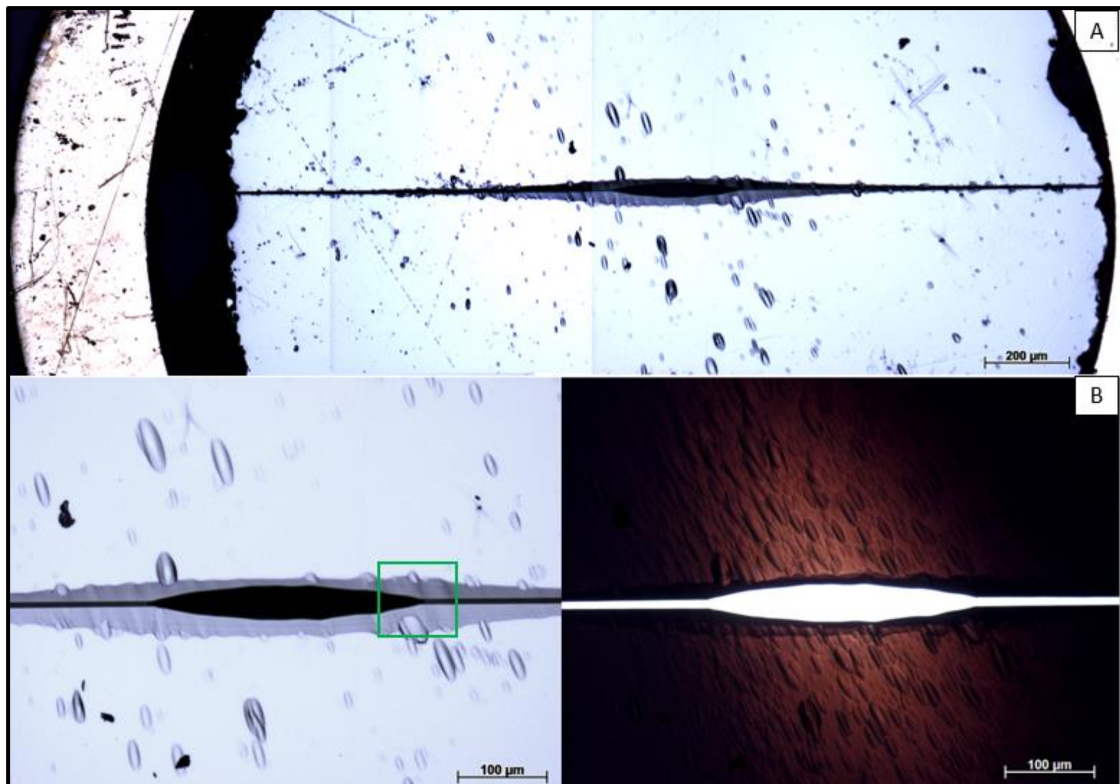

Figure 44: Light microscopy images of the Si_Sd_1 sample; A: overview, B: reflected light (left) and transmitted light image (right) with a higher magnification. A long, symmetric hole could be observed after thinning with the PIPS™. The green box marks the subsequently analysed sample position.

Only a few thinning shell-like patterns are visible on the remaining surface. It is difficult to know which position is observed in the TEM and which side of the hole must be thinned in the NanoMill® due to the symmetry of the hole. In general for silicon, it is not relevant which side is thinned, but in daily work, an interesting structure could be present, which shall undergo an additional thinning or cleaning step and this can cause problems.

In this case, the LIMI image did not help to distinguish the sample positions. *Figure 45* shows the whole sample tilted by 10° (A) and a magnification of the symmetric hole (B) in the NanoMill®.

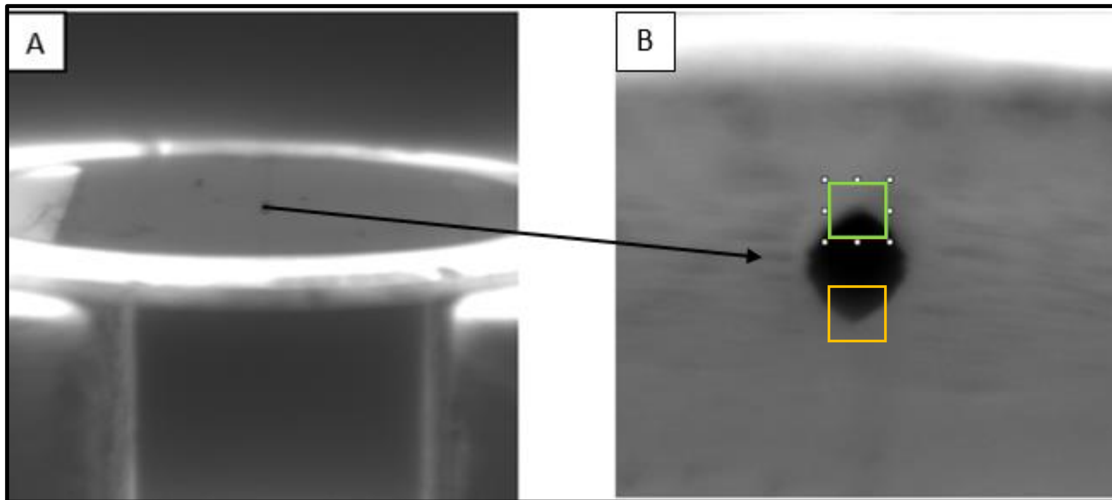

Figure 45: (A) Overview of the sample Si_Sd_1 in the NanoMill®, (B) magnification of the hole. The glue lines cannot be seen, but the symmetric hole is visible. The sample position in the green box looks exactly like the position below (orange box).

Simply two positions of the hole can be selected for thinning: the upper (green box in *Figure 45*) and the lower side (orange box), because the region of interest is the cross-section. Without additional help, it is not possible to thin and rediscover a certain position on the cross-section sample. However, there is a way to solve this problem with the reference point method dealt with later in this chapter.

Sample Si_Sdw_1

It could not be shown that the wire has any influence on planar or dimpled samples. Therefore, it is checked if the wire effects cross-section prepared samples

The *Si_Sdw_1* is prepared as described in section *3.3* and is a cross-section prepared silicon disc with a dimple on one side. A tungsten wire is fixed on top of the planar surface perpendicular to the glue lines of the cross-section. It is clamped at the PIPS™ with the glue lines parallel to the clamping. *Figure 46* shows the arrangement at the PIPS™ sample holder.

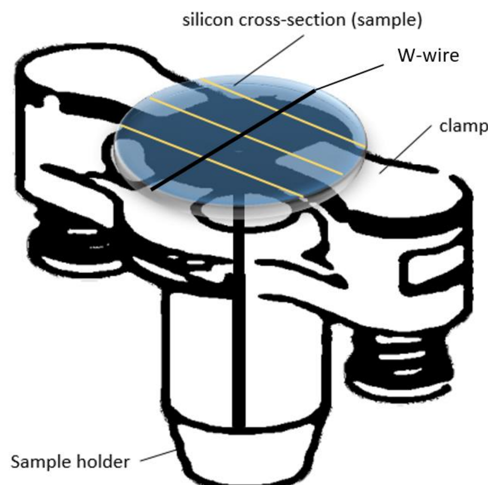

Figure 46: Sketch of the cross-section prepared sample (with tungsten wire glued on top) clamped in the PIPS^{TM} sample holder. (modified from [15])

The *Si_Sdw_1* sample is PIPS^{TM} thinned with an inspection of the preparation progress every 30 minutes. After 2 hours, milling is stopped. Looking at *Figure 47* it can be seen that the wire has an influence on the thinning result, and instead of one symmetric hole (compared with sample *Si_Sd_1*), one unsymmetrical hole possibly morphs to two holes.

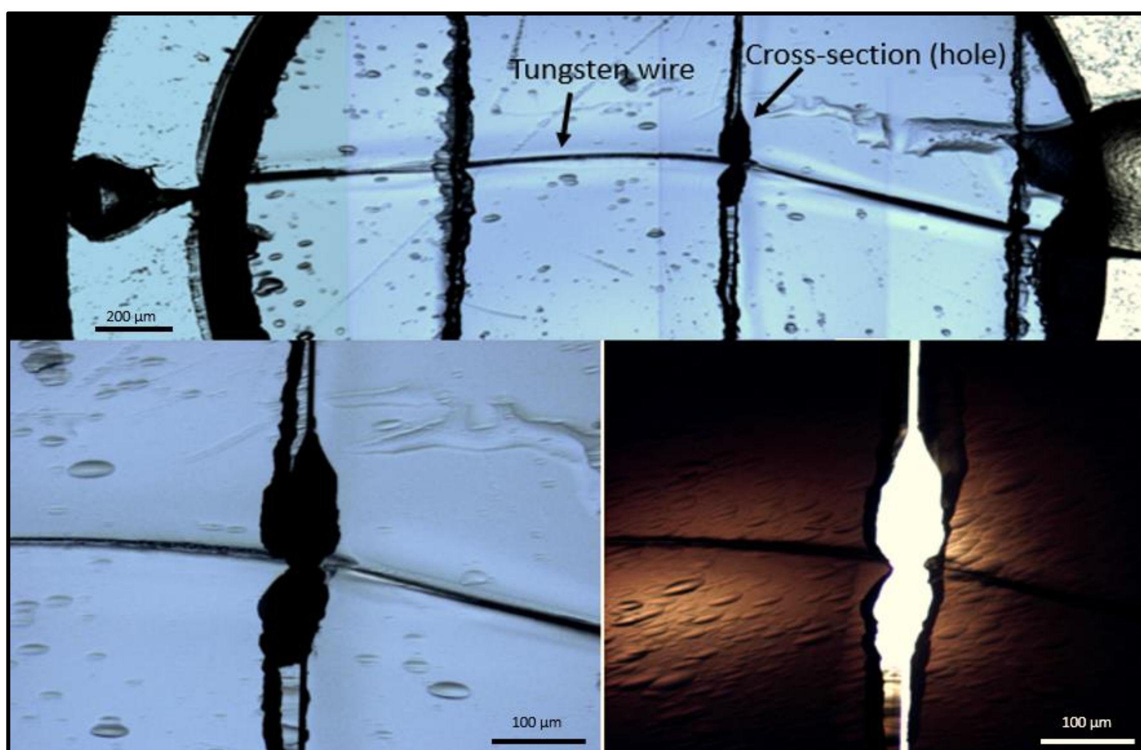

Figure 47: Light microscopy images of the Si_Sdw_1 sample; Above: an overview of the cross-section prepared sample with tungsten wire, fixed perpendicular to the glue lines after thinning in the PIPS^{TM}. Below: reflected light image (left) and transmitted light (right) with higher magnification shows evolved hole.

The advantage of the creation of the unsymmetrical hole is the possibility to find a clear position for NanoMill® thinning. *Figure 48* shows the SE image of the unsymmetrical hole which occurred during conventional thinning.

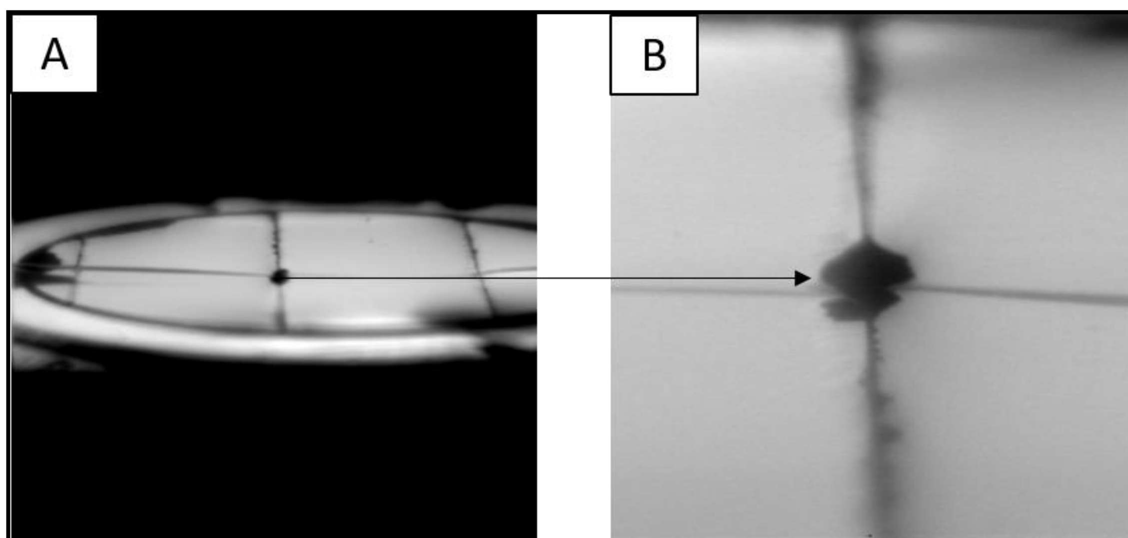

Figure 48: (A) Overview of the sample Si_Sdw_1 in the NanoMill®. The glue lines, the wire and the hole are visible. (B) Magnification of the NanoMill® image shows the unsymmetrical hole, which can be used immediately for thinning.

The same method which is used at disc prepared samples – distortion of LIMI image and comparison with the SE image (*Figure 49*) – helps to allocate the hole.

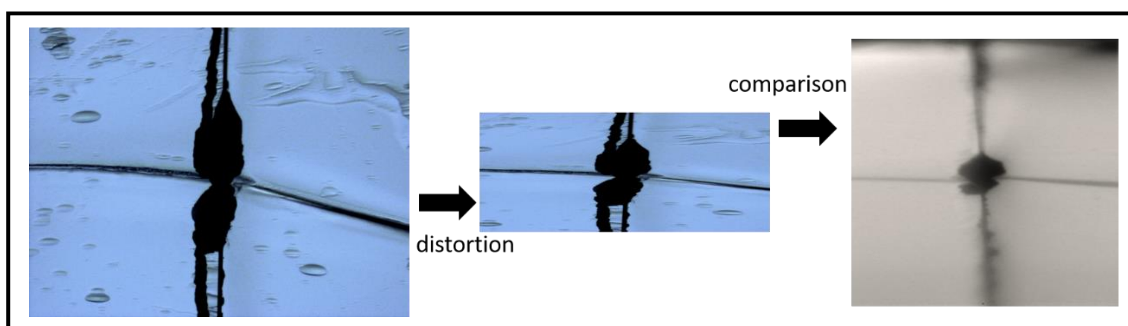

Figure 49: Distortion and comparison of the LIMI image of sample Si_Sdw_1. The unsymmetrical hole is clearly visible.

All samples and their findings are summarised in *Table 3*. The red crossed-out samples are the tungsten wire prepared planar and dimpled samples, which lead to no result. In comparison of the other samples, the preparation like *Si_Dd_1* is the best choice for disc samples and *Si_Sdw_1* for cross-section prepared samples. Due to the highly intricate preparation procedure for the cross-section tungsten wire method, the reference point method is introduced to reduce the preparation effort and time.

Table 3: Summary of all prepared samples. The crossed out samples had no effect on the thinning. The best choices are the samples in the green boxes in relation to milling time, holes and artefacts.

	Si_Dp_1	Si_Dpw_1	Si_Dpw_2	Si_Dd_1	Si_Dd_2	Si_Ddw_1	Si_Sd_1	Si_Sdw_1
sample geometry	planar disc	planar disc	planar disc	disc with dimple	disc with dimple	disc with dimple	cross-section prepared sample	cross-section prepared sample
milling time	4 h 30 min	7 h	6 h 10 min	1 h 15 min	3 h 30 min	1 h 20 min	1 h 30 min	2 h
holes	big	small holes	small holes	small holes	big hole	big hole	long symmetric hole	long unsymmetric hole
scratches	yes	yes	yes	yes	yes	no	yes	no
shell-like structure	numerous	less	less	less	few	no	few	few
cleaning artefact	no	no	no	no	yes	yes	few	no

Reference Point Method, developed for symmetric cross-section holes

If a PIPS™ hole is symmetrical, it is virtually impossible to differentiate the sides of the hole in the NanoMill® (see *Figure 45*). Consequently, an alternative approach has to be used to ensure that all consecutive analysis of the whole workflow deal with the same area. To achieve this, the desired side is marked with a waterproof pen on the brass cylinder of the cross-section sample. In the TEM sample holder, the mark points to the right side of the sample holder (see *Figure 50*).

Figure 50: The position of the marking on a cross-section sample in the TEM sample holder.

The sample is tilted 180° in the TEM during the sample lock in. Furthermore, a rotation is visible, when comparing the fluorescent screen to the image on the computer screen. Sample tilting and rotation is demonstrated in *Figure 51*.

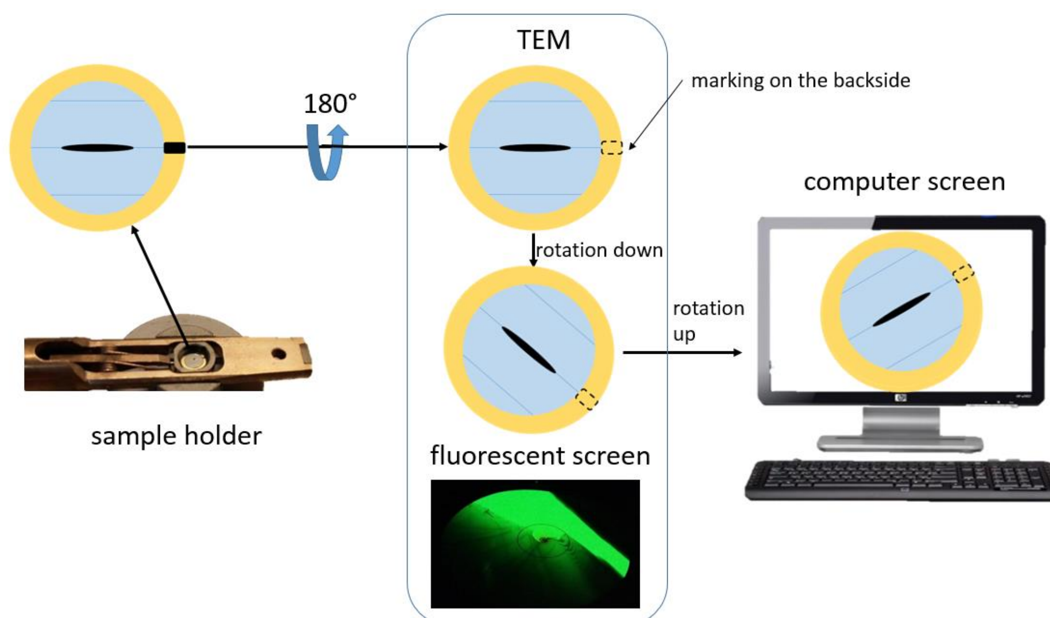

Figure 51: Sample tilting and rotation from sample inserting to imaging at the computer screen on the CM20 TEM.

It is important to know the correct position of the desired thinning area for thinning in the NanoMill®. The sample has to be positioned in its sample holder in a special direction by using the reference point method again. The same sample is taken and clamped with the mark showing up. *Figure 52* shows the approach.

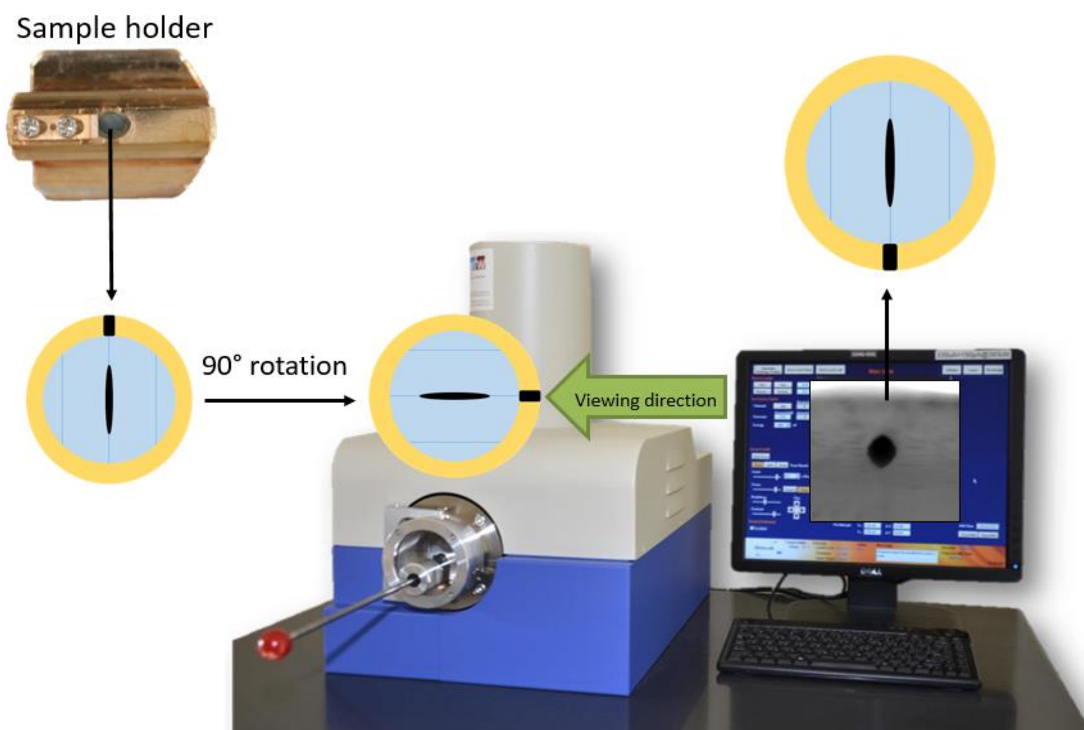

Figure 52: Sample tilting and rotation from the sample insertion to SE imaging.

To sum up: The necessary mark is made at the brass cylinder on one side of the hole. This side points towards the right side of the sample holder of the TEM. The sample position is found on the computer screen at the upper right side corner of the screen. To find and thin the desired sample position in the NanoMill®, the sample has to be locked in with the mark upwards in the sample holder. One has to keep in mind that at the user interface the bottom part of the hole must be selected for thinning (*Figure 53*).

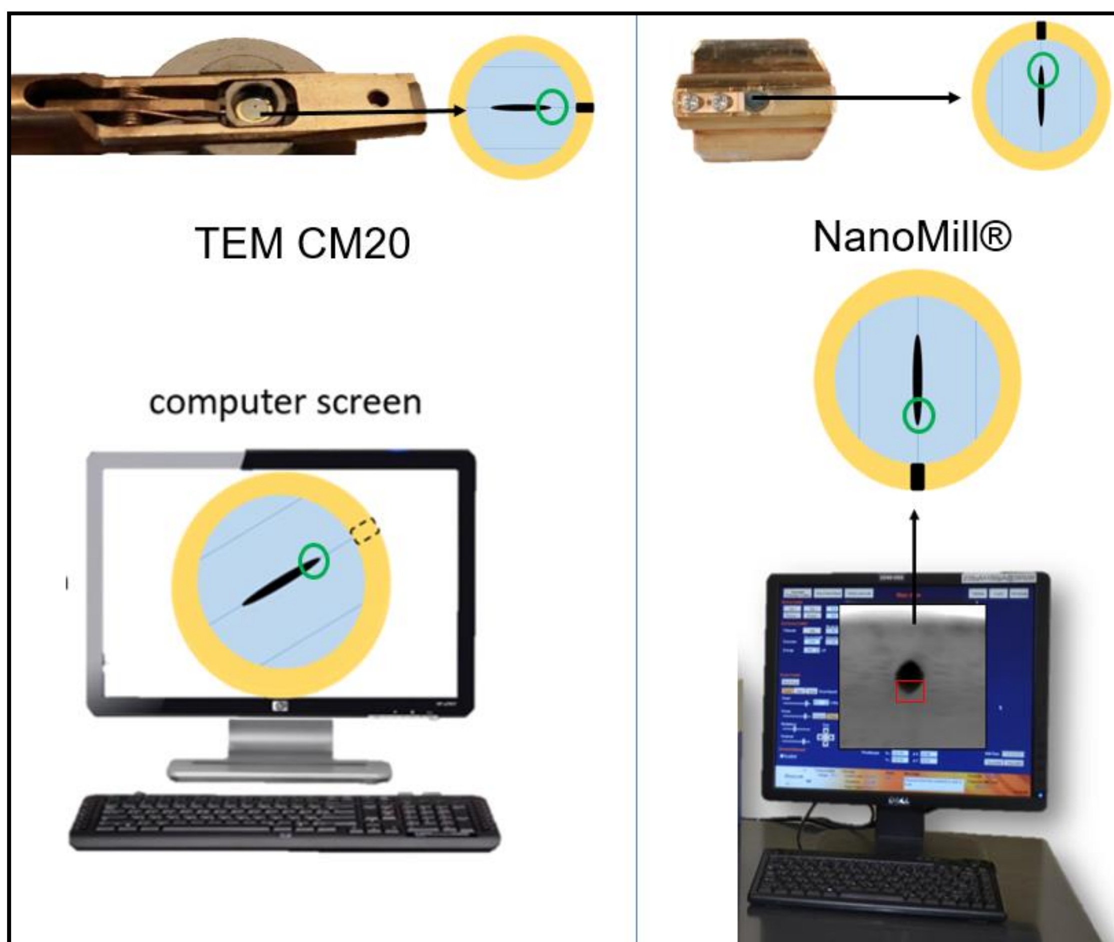

Figure 53: Overview of the reference point method, used at the TEM CM20 and NanoMill® for thinning symmetrical holes.

The reference point method enables choosing the same sample position in the TEM as well as in the NanoMill®. The result of thinning sample *Si_Sd_1* is shown in *Figure 54*.

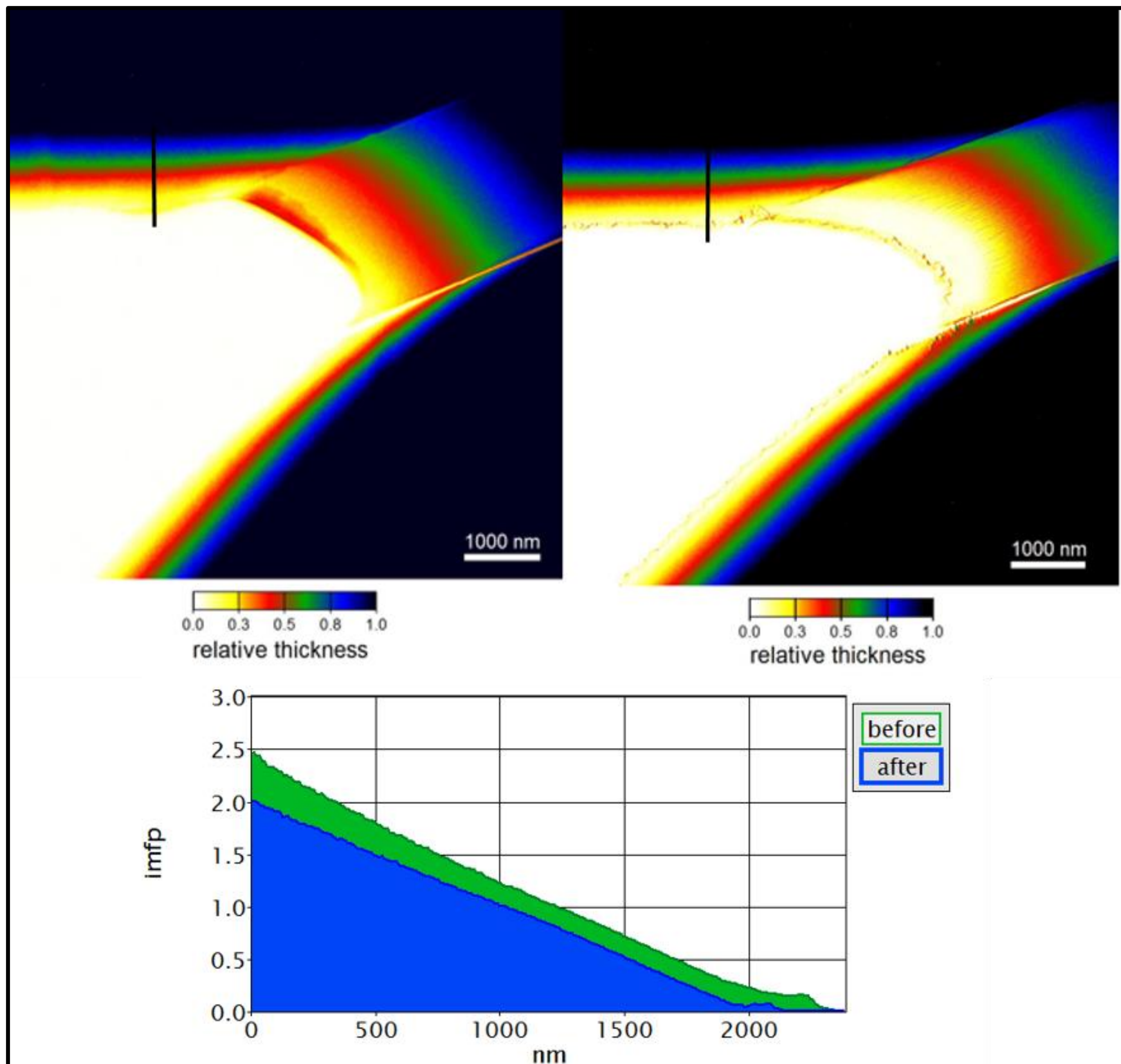

Figure 54: Si_Sd_1 t/λ map of a certain sample position before (left) and after (right) additional milling with NanoMill®. Thinning can be observed with a post-thinning factor of 1.31.

A thinning of the material is visible by comparing the thickness map before milling in the NanoMill® (left) and the thickness map after milling (right) in *Figure 54*. Additionally, the line profiles show a post-thinning factor of 1.31. Hence, the reference point method is a solution for better orientation at symmetric holes and provides a relatively simple way to avoid the preparation using the tungsten wire method.

5. Atomic Force Measurements -Beam Characterization

This part centers on the beam characterization of the NanoMill® instrument and on the removal of sputter rate evaluation for silicon. By subsequently analysing the milling results with AFM, a second, detailed inspection mechanism of the thinned regions is available, that furthermore allows the calculation of the removed material volume per time. For this, the LE ion beam profile is relevant and a setup is preferred, in which the beam hits the silicon surface perpendicularly. This prevents the beam shape observation becoming convoluted with angular incidence (*Figure 55, left*). At well focused and stigmatised beam conditions, the expected beam shape is supposed to be Gaussian, reflected by a resulting AFM profile of reversed Gauss shape from the milled cavity (*Figure 55, right*).

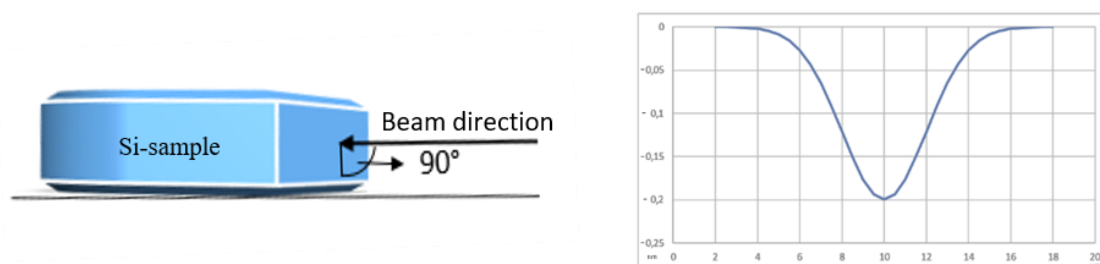

Figure 55: Beam-sample setup: sketch of the beam, which hits the surface at an angle of 90° (left) and the expected beam profile, made visible with line profiles at AFM images, should look like a reverse gauss curve (right).

For this experiment, a 3 mm disc, cut out of a silicon wafer with the ultrasonic disc cutter, is sectioned with the diamond wire saw into halves and the cross-section area is then ground and polished. Platinum crosshairs are deposited with the FIB for a better orientation and to find the milling position easier in the AFM (see *Figure 56*).

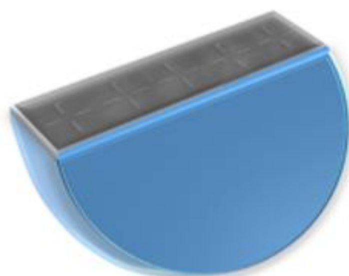

Figure 56: Sketch of a ground and polished cross-section area with platinum crosshairs, deposited in the FIB for better orientation in the AFM.

The prepared half disc is transferred to the NanoMill®, which can be set up for two different targeting options, spot milling or using a 2x2 µm targeting window. According

to the NanoMill® manual [8], spot and 2x2 µm targeting window should have the same size, expected to yield very similar milling results. The experimental parameters used for the milling procedure in the NanoMill® are listed in *Table 4*.

Table 4: Milling parameters for beam characterization

Milling Parameters	
Source Energy	900 eV
Source Emission / Beam Current	200 µA / 100 pA
Magnification	911
Milling time	30 minutes

In the AFM, height information is recorded, and the beam shape and beam diameter, as well as the depth of the milled area, can now be determined from the profiles. The results in *Figure 57* are very different and show the milling spot (left) and 2x2 µm milling area (right).

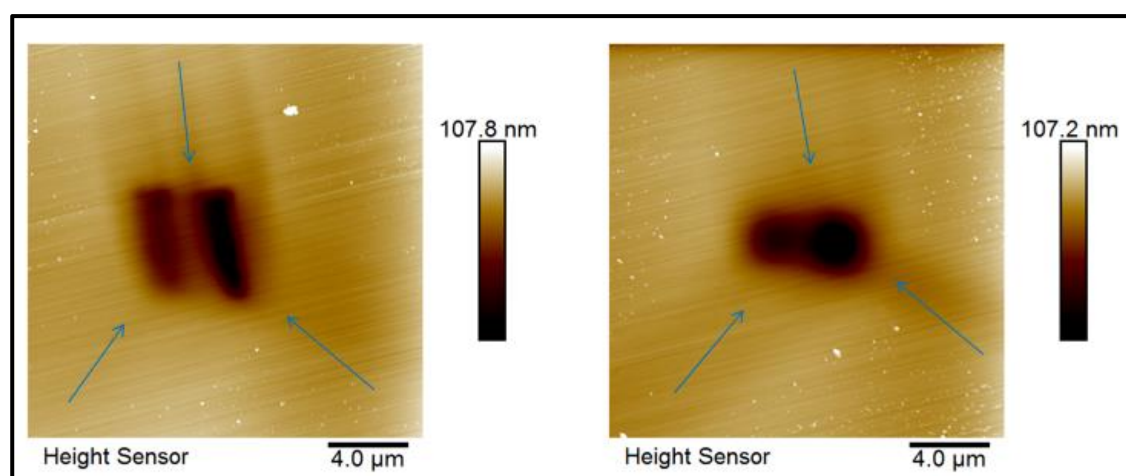

Figure 57: Resulting AFM height images: spot milling (left), 2x2 µm milling (right). The blue arrows indicate a three-fold symmetry and two milled zones instead of one appeared.

In both cases, two neighbouring zones, one milled deeper than the other, are clearly recognisable. Line profiles (see *Figure 58*) reveal quantitative difference. The depth ratio is the same in the spot milled area as well as in the 2x2 µm area, the latter being approximately 25 % deeper. The extra groove can be an indicator of the existence of a double beam misalignment. In addition, a three-fold symmetry, visible as a star shape (*Figure 57*, *blue arrows*) is observed in both images.

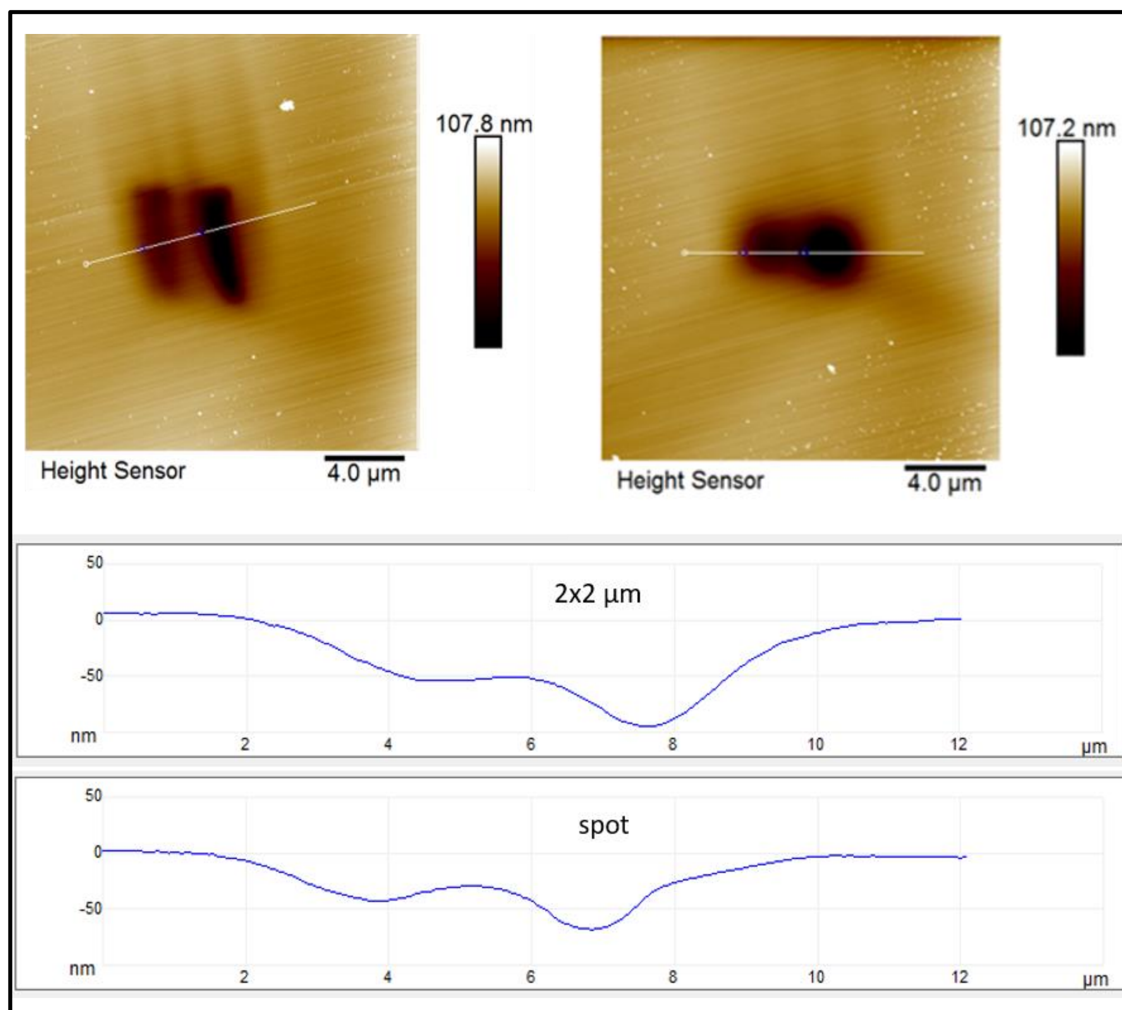

Figure 58: The lines in the AFM height images (left; spot and right 2x2 µm) indicate where a line profile is plotted. Down: Line profiles of spot and 2x2 µm area milling; the profiles show two neighbouring differently milled zones instead of the expected one milled zone with a milling profile like in Figure 55.

This unexpected result was summarised and a short report was sent to the company Fischione, requesting clarification. Meanwhile, the spot size and 2x2 µm targeting window tests were repeated to proof reproducibility. At five different places on the sample near the crosshair, spot milling and 2x2 µm area milling are carried out in the order of the numbers (*Figure 59* and *Figure 60,1-5*), to check whether the chronological order has an influence on the milling result. The source is started 30 minutes before milling in order to have a stabilised beam and astigmatism correction is done at position one for both test series. Tests are performed in the following order: (1) 30 minutes waiting time (beam stabilising), 30 minutes milling at position one, setting the targeting window to position two, (2) waiting for 30 minutes, milling 30 minutes at position two and so on. The obtained results are shown in *Figure 59* (spot milling) and *Figure 60* (2x2 µm area milling).

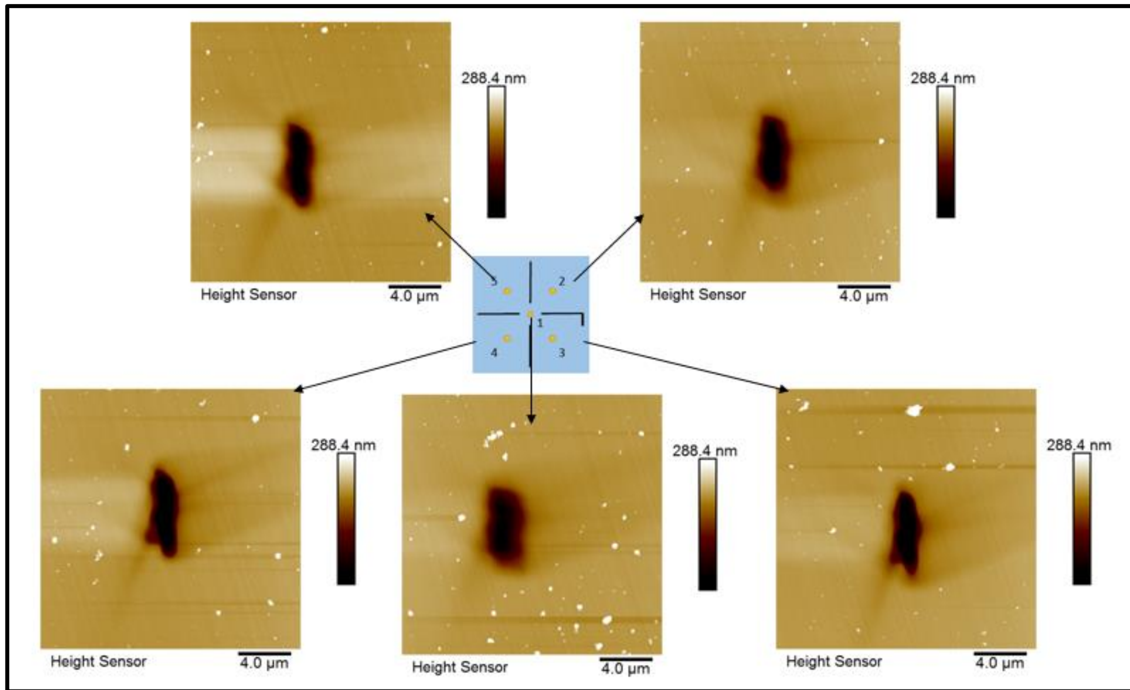

Figure 59: Spot milling: The blue box in the middle shows the spot milling positions and the milling order. The blue box is turned 90° to the right because the images are recorded like this in the AFM. The milling is done for 30 minutes each with a waiting time of 30 minutes between each milling to ensure beam stability. The shape of the beam and the depth of the milled zone are different at each test position.

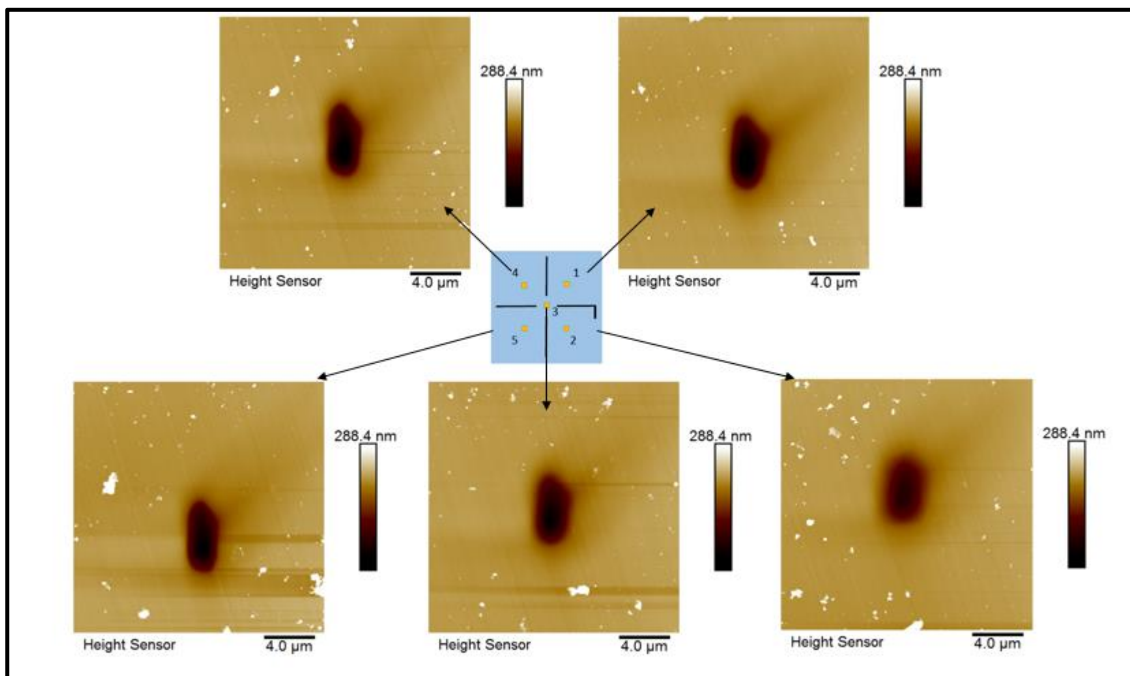

Figure 60: 2x2 µm milling: The blue box shows the milling positions and the milling order from 1-5 and the blue box is turned 90° due to the recording at the AFM. The height images show different shapes of the 2x2 µm milled region as well as different depths.

The spot depths vary from 191 nm to 281 nm and the 2x2 µm area depth varies from 150 nm to 203 nm. A beam shape change is observed throughout the five milling positions

at both experiments. No relation was found with the milling order. Hence, SEM images are taken to get more information about the milled areas (see *Figure 61*).

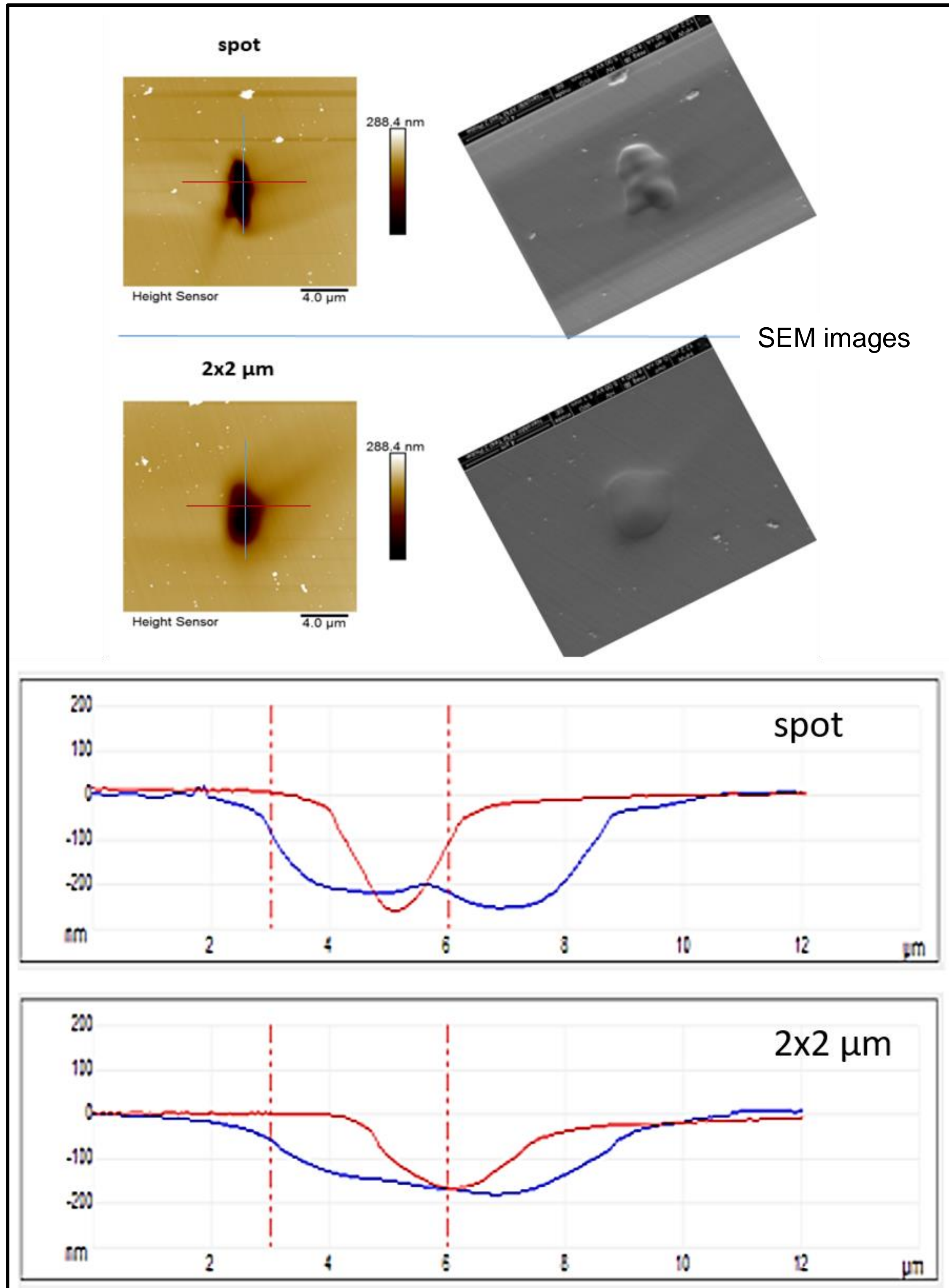

Figure 61: The AFM images give information about the depth of the milled zone, whereas the SEM images give surface information. Due to that, the SEM image visualises, that there is no homogeneous ablation of the material. Looking at the red (horizontal) and blue (vertical) line profiles, this inhomogeneity can be seen: there are two neighbouring deep milled zones like in the first test (Figure 58).

The repetition of the tests could not explain the performance of the ion beam. In the meantime, Fischione admitted a software problem and arranged the reprogramming of the scanning firmware. After the software update (Version 3), the tests were repeated in the presence of the service technician. The AFM height images, which are generated after milling with the new software (*Figure 62*), showed no improvement in the behaviour of the ion beam. Even after software installation, the ion beam did not show a defined shape.

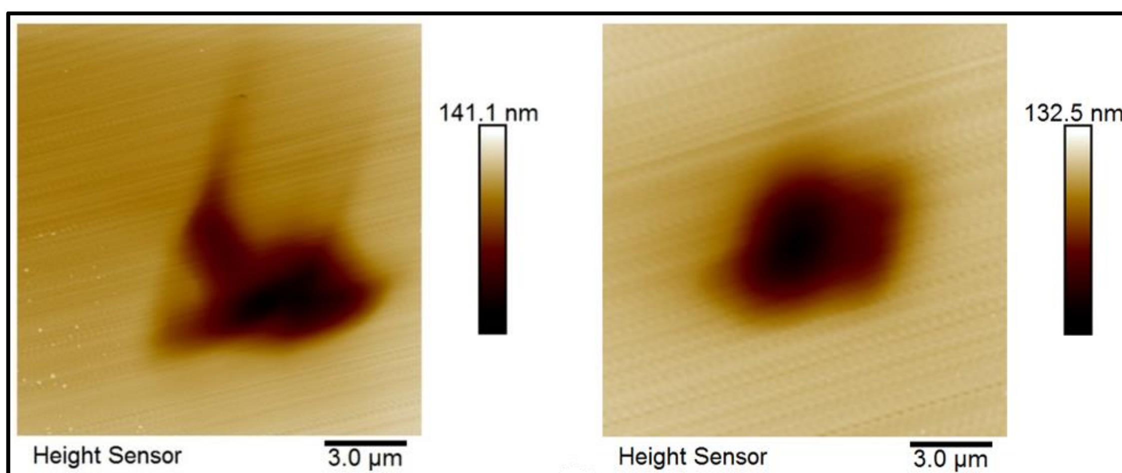

Figure 62: AFM height images: spot milling (left) 2x2 µm area milling (right) after the software update. The milling result is similar to the outcomes before. No improvement of the beam can be observed.

Due to this result, an extra test was carried out to check whether this non-spot shape might be due to surface charging. To exclude this possibility, the test sample is sputtered with a thick layer of Au/Pd, and the spot milling test is repeated. The resulting height image in *Figure 63* shows that the beam shape is neither improved nor remotely spot-like and therefore surface charging could be excluded.

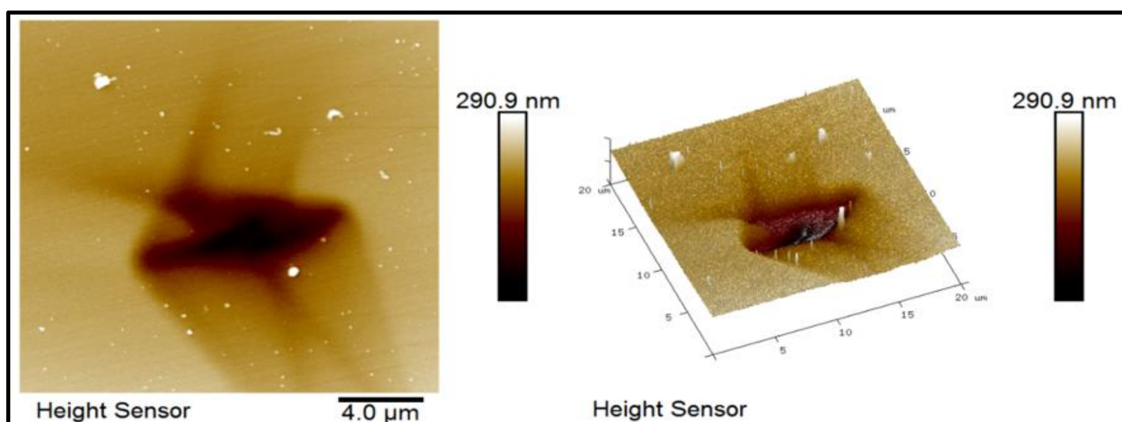

Figure 63: Spot milling test on an Au/Pd sputtered Si sample testing if surface charging matters. The milled area shows approximately the same shape as seen before for the Si surface in Figure 62.

It then came down to further analysis of the electrical setup of the beam deflection coils, deemed to be not properly configured. This is still an ongoing issue and it has to be sorted out whether this is related to hardware or software problems.
Dealing with this pragmatically, in the next test, an area of 20x10 µm, which is used as standard targeting area for the milling of FIB lamellae (recommended by Fischione) is chosen to determine, how the undesired beam shape and scan behaviour affects the thinning of these lamellae.

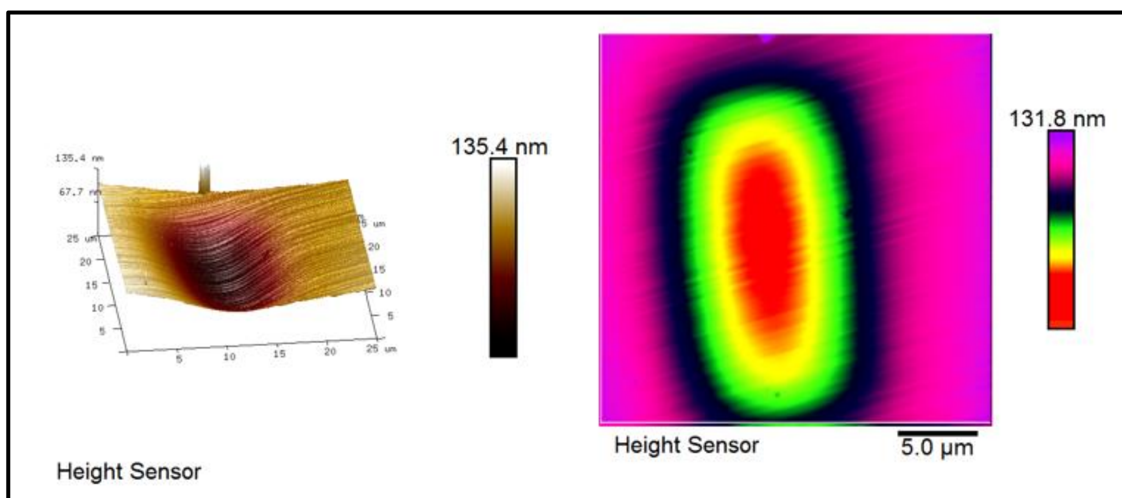

Figure 64: 3D height images of the 20x10 µm milling area, which shows a bathtub shape (left), height images coloured to show irregular milling inside the (red) 20x10 µm milling box (right).

The shape of the received AFM image is approximately the shape of the selected thinning area, but no uniform thinning is observed. Different heights are indicated by different colours according to the colour bar in *Figure 64* to point out the resulting flatten bathtub shape and the resulting inhomogeneous thinning.
In order to visualise the effects of the ion beam on the silicon sample under usual milling conditions (*Figure 65, left*), a final experiment is carried out with an incident ion beam angle at 10° on a flat silicon surface (*Figure 65, right*).

Figure 65: Usual milling conditions for FIB lamellae (left), test on Si sample with +10° tilt (right) to simulate the conditions for AFM measurements.

A milling area of 5x5 µm and milling time of 60 minutes are chosen instead of a 20x10 µm targeting window to reduce the test time and to catch a measurably milling depth for the AFM tests.

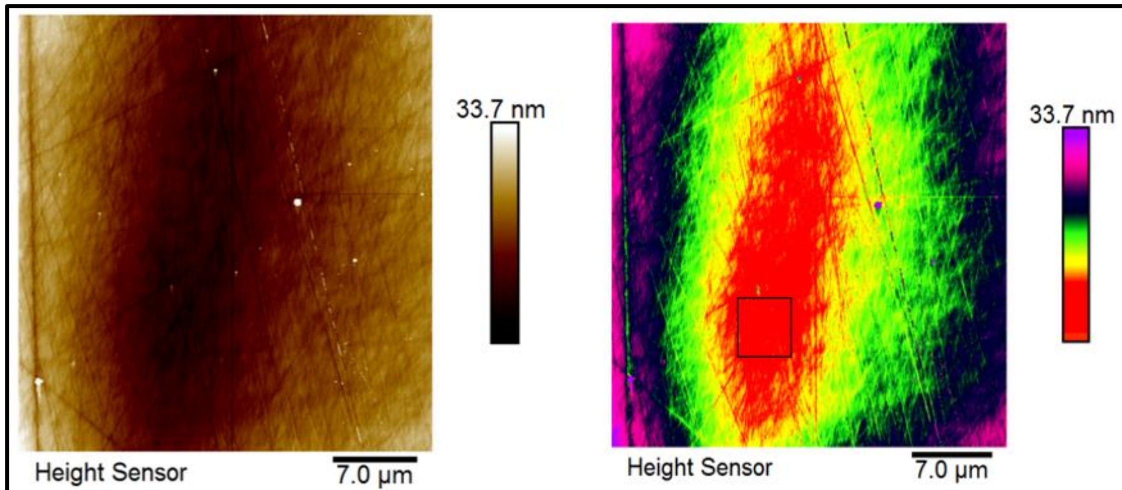

Figure 66: Result of 5x5 µm milling under usual milling conditions. A lateral elongation of the milling area can be observed, which is visualised in colours (right). The black box marks the 5x5 µm milling area.

In general, one would expect a milled shape in the size of 6x6 µm containing 5x5 µm milling area plus 1 µm at each side because of the beam size. The visible elongation in *Figure 66* (black box marks the 5x5 µm milling area) results due to the +10° tilting of the sample. Same as in the 20x10 µm experiment, the thinned area is significantly wider than the expected 5x5 µm. *Figure 67* demonstrates the result of the same test, performed at an incident beam angle of 90°, where no elongation is apparent –In principle, the elongation is negligible during lamellae milling in the NanoMill®, because the milling pattern is set in a way that this elongation ends in the vacuum. The milling area itself seems more uniform than the milling area at the 20x10 µm test.

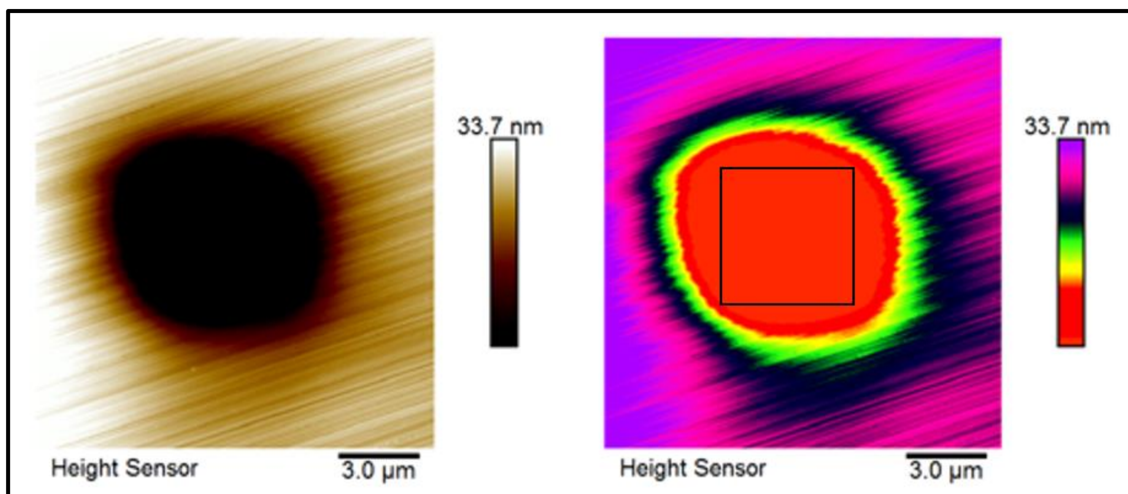

Figure 67: Same experiment as in Figure 64, but the incident beam angle is set at 90°. The black box marks the 5x5 µm milling area (right) and no elongation is observed.

To illustrate the effects of the milling with a 20x10 µm and 5x5 µm pattern with an angle of incidence of 90° (*Figure 68*), the milling patterns and the measured areas affected by

the milling were schematically placed on a lamella of the standard size (10x5 µm). The black boxes mark the selected milling area and the red ones the affected milling area. The thinned region is larger than the milling pattern size in both cases.
In practice, the milling pattern is set in the NanoMill® in a way that the pattern covers half of the lamella. Choosing a 20x10 µm pattern, which is the usual milling pattern for lamella thinning (recommended by Fischione Instruments), it is visible that the milling in the selected pattern is not as homogeneous as wanted and the red area is too close to the grid. In this configuration, the grid would be thinned too, which causes unwanted re-deposition. Looking at the 5x5 µm setup, the red area is far enough away from the grid, so that uniformly thinning without re-deposition from the grid is ensured.

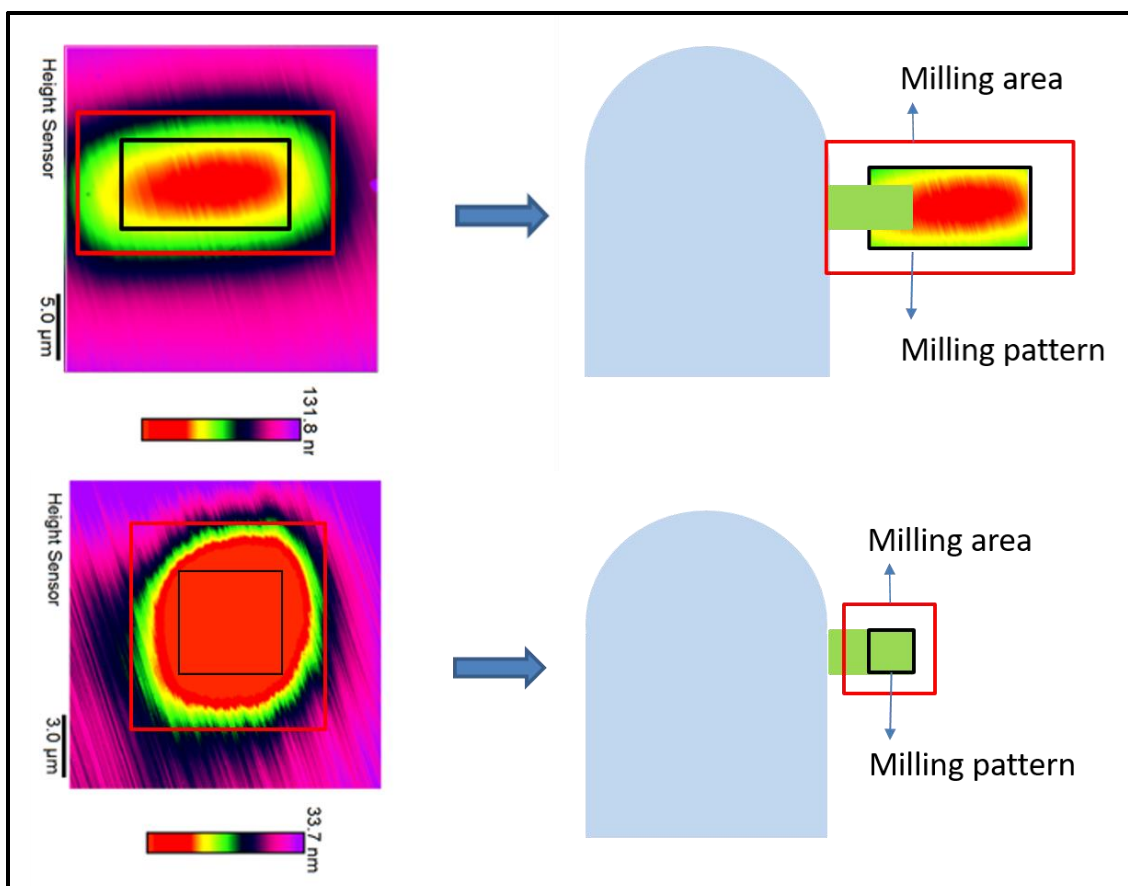

Figure 68: Above: The black box shows the selected milling area (20x10µm) and the red box marks the area, where the milling is significant (16x30 µm). On the right side is a sketch of a lamella with the setting of the boxes. Below: The same case for a 5x5 µm milling area (black box) with significant milling area (red box, 10.5x10.5 µm).

To get a uniform thinning despite the beam shape, the pattern has to be as small as possible to avoid re-deposition by thinning the grid. Furthermore, it has to be quadratic, because with the length the milling area gets more inhomogeneous, (like the 20x10 µm pattern shows).

Based on the existing data and due to the unreliable beam behaviour and resulting beam shape, it was not possible to calculate a removal rate for silicon within the timeframe of this master thesis. However, further work together with the manufacturer will be done to clarify the issues.

6. Conclusion

The goal of this master thesis was finding the conditions and estimating the effort for low-energy ion thinning and relocating defined sample positions from mechanically pre-prepared and conventionally ion milled TEM samples.

A useful workflow is introduced, correlating TEM, LIMI and SE imaging, to allow low energy argon ion milling of a defined area on samples that have been differently pre-treated by standard mechanical preparation such as planar, dimpled or cross-section preparation. The tests showed that it is preferential to generate many small holes over just one big hole for a more efficient LE post treatment. Dimpled samples are preferred due to a shorter milling time and less preparation induced artefacts.

In view of the obtained results, where the wire did not affect the hole forming process, it is of particular importance to fix the tungsten wire in the centre of planar and dimpled samples. This can be achieved by LIMI guidance in transmission, where it is possible to recognise the thinnest region. The best thinning is provided on samples free of scratches, being as clean as possible. The findings for planar and dimpled samples are also valid for cross-sectioned samples. There, the problem is to identify the desired sample position along the long, symmetric hole, appearing during PIPS™ thinning. The application of a tungsten wire on a cross-section sample tended to form two holes at different places. Such a sample can be used directly for thinning at low energies because of the irregular shape hole. The time-consuming tungsten wire method can be avoided by involving the reference point method in combination with cross-section preparation. Based on those findings, it is recommendable to produce dimpled discs with small holes as scratch free and clean as possible or dimpled cross-section prepared using reference points.

The characterization of the milling behaviour of the NanoMill® instrument by means of AFM measurements were less successful, due to insufficiencies in software and possibly hardware. Tests of spot and area milling are performed and results show the existence of a double beam (two neighbouring milled zones, differently deep milled) and a three-fold symmetry, preventing the determination of the removal rate for silicon. Furthermore, the standard targeting window (20x10 µm) for FIB lamellae milling is analysed to determine, if the undesired beam shape affects the thinning. Unfortunately, no uniform milling is observed. The milling area is larger than the pattern size and a flatten bathtub shape occurred. The influencing parameter is the pattern size: rectangular milling patterns lead to inhomogeneous milling of FIB lamellae. As a result, the targeting window has to be quadratic and as small as possible in order to get uniform thinning despite the beam shape.

Bibliography

[1] J. Ayache, ed., *Sample preparation handbook for transmission electron microscopy: methodology*. New York: Springer, 2010.

[2] D. B. Williams und C. B. Carter, *Transmission electron microscopy: a textbook for materials science*, 2nd ed. New York: Springer, 2008.

[3] R. R. Cerchiara *u. a.*, „Raising the Standard of Specimen Preparation for Aberration-Corrected TEM and STEM“, *Microsc. Today*, Bd. 19, Nr. 01, S. 16–19, Jan. 2011.

[4] M. Mitome, „Ultrathin specimen preparation by a low-energy Ar-ion milling method“, *Microscopy*, Bd. 62, Nr. 2, S. 321–326, Apr. 2013.

[5] K. A. Unocic, M. J. Mills, und G. S. Daehn, „Effect of gallium focused ion beam milling on preparation of aluminium thin foils: EFFECT OF GALLIUM FIB MILLING ON PREPARATION OF ALUMINIUM THIN FOILS“, *J. Microsc.*, Bd. 240, Nr. 3, S. 227–238, Dez. 2010.

[6] Fischione Instruments Inc., „Model 1040 NanoMill ® TEM specimen preparation system - Specimen configuration“. Juli-2012.

[7] R. Seidl, „Specimen Preparation for Transmission Electron Microscopy by Focused Ion Beam: Refinement of Post-Treatment using Focused Low Energy Argon Ion Milling“, Diplomarbeit, Technische Universität Graz, Graz, 2016.

[8] T. Ghosh, M. Bardhan, M. Bhattacharya, und B. Satpati, „Study of inelastic mean free path of metal nanostructures using energy filtered transmission electron microscopy imaging: MEASURING INELASTIC MEAN FREE PATHS USING ELECTRON ENERGY LOSS SPECTROSCOPY“, *J. Microsc.*, Bd. 258, Nr. 3, S. 253–258, Juni 2015.

[9] B. F. Vieweg, „Entwicklung und Anwendung neuartiger Präparationsverfahren für die Transmissionselektronenmikroskopie von dünnen Schichten, Nanopartikeln und Kristalldefekten“, Friedrich-Alexander-Universität Erlangen-Nürnberg (FAU), 2012.

[10] J. P. McCaffrey, „Small-angle cleavage of semiconductors for transmission electron microscopy“, *Ultramicroscopy*, Bd. 38, Nr. 2, S. 149–157, Nov. 1991.

[11] B. Schmidt und K. Wetzig, *Ion beams in materials processing and analysis*. Wien ; New York: Springer, 2013.

[12] A. Barna, B. Pécz, und M. Menyhard, „Amorphisation and surface morphology development at low-energy ion milling“, *Ultramicroscopy*, Bd. 70, Nr. 3, S. 161–171, Jan. 1998.

[13] „Gatan, Precicion Ion Polishing System Owner’s Manual and User’s Guide“. .

[14] S. M. Neumayer, „Wedge Polishing as Sample Preparation Method for Transmission Electron Microscopy: A Systematic Study“, Technische Universität Graz, 2012.

[15] „Precision Ion Polishing System (PIPS™) Model 691“. .

[16] M. J. Süess, E. Mueller, und R. Wepf, „Minimization of amorphous layer in Ar+ ion milling for UHR-EM“, *Ultramicroscopy*, Bd. 111, Nr. 8, S. 1224–1232, Juli 2011.

[17] I. G. Brown, Hrsg., *The physics and technology of ion sources*, 2nd, and extended ed Aufl. Weinheim: Wiley-VCH, 2004.

[18] M. A. Tribe, M. Eraut, und R. K. Snook, *Light microscopy*. Cambridge [Eng.] ; New York: Cambridge University Press, 1975.

[19] M. Volgger, „Lichtmikroskopie Theorie und Anwendung“. 29-Feb-2008.

[20] G. Kothleitner, „Lecture script of Electron microscopy“, Semester 2016-2015.

[21] H. Ibach und D. L. Mills, *Electron energy loss spectroscopy and surface vibrations*. New York: Academic Press, 1982.

[22] R. F. Egerton, „Quantitative Analysis of the Energy-Loss Spectrum“, in *Electron Energy-Loss Spectroscopy in the Electron Microscope*, Boston, MA: Springer US, 1986, S. 229–289.

[23] R. García, *Amplitude modulation atomic force microscopy*. Weinheim: Wiley-VCH-Verl, 2010.

[24] N. R. U.S. Army Soldier Systems Command Development, and Engineering Center Atomic Force Microscopy/Scanning Tunneling Microscopy (AFM/STM) Symposium, S. H. Cohen, M. T. Bray, und M. L. Lightbody, *Atomic force microscopy/Scanning tunneling microscopy*. 1994.

[25] T. E. Conners und S. Banerjee, Hrsg., *Surface analysis of paper*. Boca Raton: CRC Press, 1995.

[26] H. Plank, „Materials Characterization III“, 2014.

[27] S. B. Newcomb, C. B. Boothroyd, und W. M. Stobbs, „Specimen preparation methods for the examination of surfaces and interfaces in the transmission electron microscope“, *J. Microsc.*, Bd. 140, Nr. 2, S. 195–207, Nov. 1985.

[28] D.V.Sridhara Rao;K.Muraleedharan;C.J.Humphreys, „TEM specimen preparation techniques“.

[29] „Gatan Ultrasonic cutter“. 10-Nov-2016.

[30] J. Ayache, ed., *Sample preparation handbook for transmission electron microscopy: techniques*. New York: Springer, 2010.

[31] „Gatan Dimple Grinder Model 656 User’s Guide“. Nov-1998.

[32] J. H. Fitschen, J. Ma, und S. Schuff, „Removal of curtaining effects by a variational model with directional forward differences“, *Comput. Vis. Image Underst.*, Bd. 155, S. 24–32, Feb. 2017.